NTNU – Trondheim
Norwegian University of
Science and Technology

Reducing sub-harmonic spatial fields in Concentrated winding machines using Genetic Algorithms

Thomas Nordaunet

Master of Science in Electric Power Engineering
Submission date: June 2013
Supervisor: Robert Nilssen, ELKRAFT
Co-supervisor: Astrid Røkke, ELKRAFT

Norwegian University of Science and Technology
Department of Electric Power Engineering

Reducing sub-harmonic spatial fields in Concentrated winding machines using Genetic Algorithms

Thomas Nordaunet, Student NTNU, Prof. Robert K. Nilssen, NTNU, Astrid Røkke, Ph.d candidate NTNU

***Abstract*—Certain slot/pole combinations in fractional slot winding machines with concentrated coils exhibit high amount of sub-harmonic spatial fields. These harmonics may cause additional losses and ripple torque. Literature suggest solutions to reduce the amount of sub-harmonics by increasing the number of layers, varying the numbers of turns per coil or introducing flux barriers in the yokes of the machine.**

This article presents solutions to minimize sub-harmonics in a 24 slot 22 pole fractional slot winding machine with concentrated coils. A Genetic Algorithm is used to optimize the design of multiple layer windings with different turns per coil and implementation of flux barriers in the yokes of the machine. The proposed solutions are verified with Finite Element Analysis and compared with respect to sub-harmonic content, losses and ripple torque.

Fourier transform of the analytical Magnetomotive Force produced by the winding is used to characterize the sub-harmonic content. A Genetic Algorithm optimizes the winding layout using multiple partial fitness functions. Both double layer and single layer winding constraints are implemented to construct different layouts. Flux Barriers are implemented using Finite Element Analysis and Magnetic Equivalent Circuits to optimize the design and arrangement.

Calculations revealed a 85 % decrease in the 1.th sub-harmonic using the double layer windings proposed by the Genetic Algorithm, and a 46 % reduction in solid losses compared to the single layer case. A four layer winding completely removed the sub-harmonic content in the machine, consequently decreasing the solid losses by 63 % compared to the single layer case.

By optimizing the winding layout it is possible to completely remove the sub-harmonics. However, this complicates the winding layout, thus application specifications will govern the solution chosen. Flux barriers presents a simple and promising solution reducing sub-harmonics.

I would like to thank my supervisor Professor Robert Nilssen and co-supervisor Astrid Røkke at the department of Electric Power Engineering for their invaluable assistance during my thesis. I would also like to thank Smart Motor AS for providing a interesting thesis problem and sharing their design parameters.

I. Introduction

A. Context and Problem description

This is the master thesis written by Thomas Nordaunet at the Norwegian University of Science and Technology (NTNU) department of Electric Power Engineering in the spring of 2013. It is an extension of a project performed in the fall of 2012, the scope of which was field and power loss calculations in 2D and 3D FEA, with the goal to accurately model and calculate losses occurring in a specific machine built by Smart Motor AS. Sub-harmonic spatial fields due to the winding layout where found to be a source of additional power losses.

The present work extends this former work in reducing and removing sub-harmonic spatial fields by applying different methods, including research on different winding layouts and introduction of Flux Barriers in iron structures. Within these methods a number of individual variations exist, some more successful than others. To find an optimal solution, a direct analytical approach is unavailable due to the complex behaviour of such phenomena. As a consequence, numerical optimization tools are applied. Numerical optimization can be performed with numerous tools, each dependent on the solution space and problem formulation. This article focuses on using Genetic Algorithms (GA) as the optimization tool due to the discontinuous solution space of the problem. GA has proven successful in finding a global optimum in non-linear and discontinuous problems with multiple local optimums [1]. Traditional line search methods has a high probability of converging on a local optimum, and multiple initial starting values must be considered before the best solution is found. Consequently, GA is deemed a

more attractive tool for this type of optimization problem.
The article limits the scope of the applied methods to a single machine topology, the fractional slot machine with 24 slots 22 poles, 3 phases and concentrated coils.

B. Previous work

Previous work on the subject include [2], where GA is applied to automate the winding design. The multi objective fitness functions include maximizing the fundamental harmonic in the Magnetomotive Force (MMF), minimizing the sum of harmonic in the MMF and balancing the winding. Constraints such as number of layers in each slot are imposed to ensure the winding feasibility. Results indicate that the algorithm converged to the known winding layouts found in design tables for integral slot winding, and for fractional slot windings the algorithm produced a less unbalanced winding with slightly lower harmonic content compared to recommended layouts. [3] uses GA to optimize the winding layout in concentrated winding machines with the objective to reduce the amount of sub-harmonics produced. The method used is the Fast Fourier Transform (FFT) on the 1-D plot of the MMF produced by the winding. Five partial fitness functions are used in the objective function, minimizing harmonics and maximizing the winding factor. Results demonstrated a complete removal of sub-harmonics although the winding factor was low. Only four layer winding solution were presented. [4] presents variations regarding Flux Barriers in the stator yoke of a 12 slot 10 pole concentrated coil machine, and presented a resulting reduction in sub-harmonic content. [5] presents five variations regarding the placement of flux barriers in a 36 slot 34 pole machine with single layer windings. Different combinations include flux barriers in the stator yoke, flux barriers below the rotor magnets and a thinner rotor yoke. Only stationary FEA was performed, and uncertainty about the time and rotational aspect was not investigated. Regarding the Total harmonic distortion (THD), the best solution found was a 6+6 sectioning of the stator yoke and a sectioning of the rotor beneath each magnet.

C. Objectives and Method

This article aims at using GA to reduce sub-harmonic spatial fields in a fractional slot winding machine with concentrated windings. Two methods, multiple layer winding and flux barriers, are used to directly and indirectly influence the amount of sub-harmonics in the machine. For the 24 slot 22 pole machine, two and four layer windings with different number of turns per coil has not been investigated earlier. This article also aims at creating custom crossover and mutation functions always creating feasible offspring, eliminating the need for penalty functions and repair algorithms. This will improve the speed and coverage of the search space.
Optimizing the placement and width of flux barriers with the use of GA are performed. FEA software and Magnetic Equivalent Circuits (MEC) are used in computing the harmonic spectrum, thus connecting the GA with FEA and MEC. Earlier research on GA connected with FEA software or MEC regarding optimization of flux barriers has not been found, making this a state-of-art optimization procedure.
First, the basic theory regarding winding layout, sub-harmonics and losses are presented, second, the theory on GA, third, the FEA and MEC models used are presented, fourth the GA and custom GA functions, fifth a collection of the results and lastly a discussion and conclusion on the reported findings.

II. Theory

A. Fault tolerance

Fractional slot machines with concentrated coils have gained much attention in application where the risk of fault operation is high. Such operation include the occurrence of short circuits in the system or the ability to function when normal operation is not possible. During a short circuit, the fault current may be limited to prevent damage to equipment, by introducing a high phase inductance [6]. Operation outside of the normal range include operation with open-circuit or short-circuited phases. The requirement on a fault tolerant system is:

- phase redundancy
- physical separation of phases
- high phase inductance
- low mutual inductance

Phase redundancy require electrical separation between the phases, or possibly each coil, by the use of special drives topologies [7]. As a consequence a faulty phase does not interfere with the other electrical components.

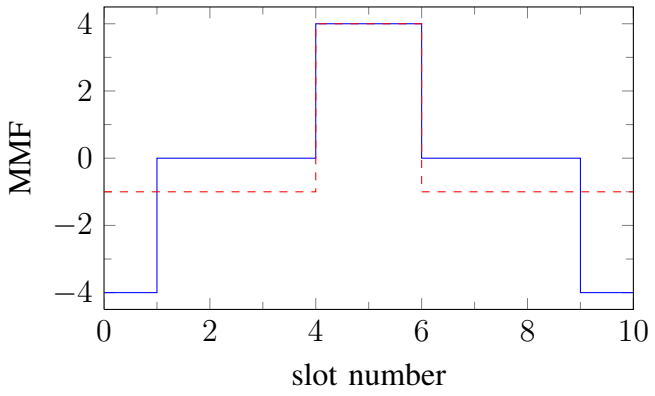

Fig. 1. Magnetomotive force produced by one phase in a 10 slot machine. Coil throw is two slot pitches. Red dashed; phase winding with one coil. Note the non-zero value over the other slots. Blue; winding with two coils. Note the zero value over the other slots.

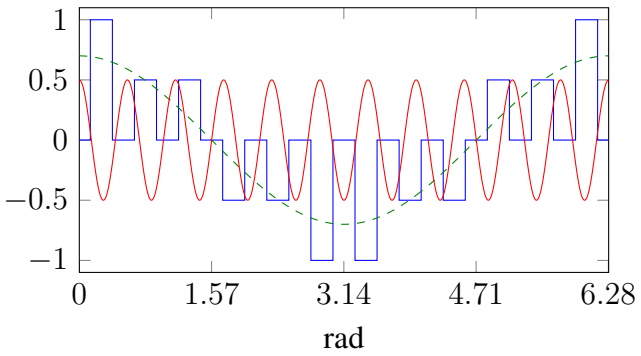

Fig. 2. MMF distribution of a 24 slot 22 pole machine with single layer concentrated coil winding. Blue lines are the idealized MMF at one instance of time when symmetrical currents are applied to all the phases. Red = Main harmonic $\nu = 11$. Green (dashed) = Fundamental harmonic $\nu = 1$.

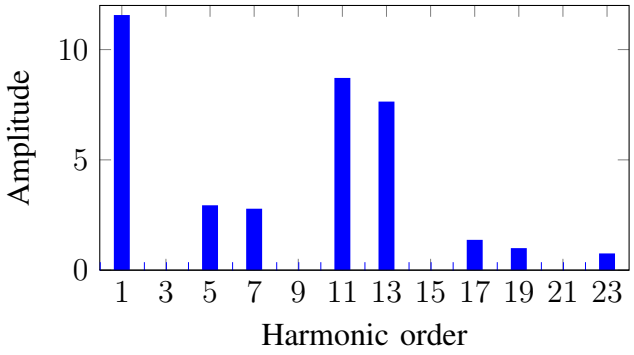

Fig. 3. Harmonic spectrum of MMF in Fig. 2. Only odd harmonics are present. Harmonics orders of multiple of $m = 3$ cancels.

A *physical separation* of the coils can be achieved by introducing concentrated coils (CC) where the end windings do not overlap, preventing a phase to phase fault. Single layer windings where each slot only contain one phase is especially redundant to this type of fault.

High phase inductance limits the short circuit current in the machine and system. Inductance is a design parameter governed by the winding layout and geometrical shape of the machine. *Low mutual inductance* between the phases minimize the reduction in performance in the healthy phases during a fault [6]. This is mainly guided by the winding layout [8].

Mutual inductance is evaluated by studying the Magnetomotive Force (MMF) produced by each phase. According to Amperes law, the MMF is the cumulative sum of the number of turns in each slot along the circumference of the stator. Fig.1 shows the MMF produced by two winding layouts for a 10 slot machine. In one layout, marked with dashed line, the MMF is non-zero in between the coil. This non zero flux links the two other phases creating a strong mutual inductance. The second layout, marked with solid line, shows a winding layout with two coils. Here, the cumulative sum is zero in between the slots of one phase. Another phase coil placed in any of these slots will create a zero mutual inductance.

B. Sub-Harmonic fields

Spatial harmonics are magnetic fields generated by the winding layout and the finite number of slots and conductors in the machine. Since a machine has moving parts and time-variant electric currents, spatial magnetic fields are generated with frequency in both time and space. Fig. 2 displays a MMF plot of a single layer winding layout for a 24 slot 22 pole machine. Blue lines indicate the idealized case of the MMF produced by a symmetric current in all the three phases at one instant of time. According to Fourier series, any signal can be composed of the sum of sinusoids with different amplitude and frequency. Calculating the Fourier series, the spectrum in Fig. 3 is obtained, showing the amplitude of each harmonic in the MMF. A 22 pole machine creates a working torque with harmonic order equal to the 11.th, shown in red in Fig. 2. This harmonic is called the main harmonic. The 1.st harmonic, seen in dashed red and called the fundamental harmonic. Others below the main harmonic are known as a sub-harmonics.

C. Losses

Induced currents and core losses are objectives in establishing a qualitative measure for comparing the different methods analysed. In general, three losses could be defined, one is eddy current losses, a consequence of time varying flux densities in conductive materials:

$$\nabla \times \mathbf{E} = -\frac{\partial \mathbf{B}}{\partial t} \tag{1}$$

$$\mathbf{J} = \sigma \mathbf{E} \tag{2}$$

$$P = \int_V \sigma \mathbf{E}^2 dV \tag{3}$$

$\mathbf{B}$ is the flux density vector, $\mathbf{V}$ is the electric field vector and $\mathbf{J}$ is the current density vector. Eddy current losses in non laminated conductive material becomes:

$$P = \frac{1}{\sigma} \int_V J^2 dV \tag{4}$$

Where V is the domain and σ is the conductivity of the material. (4) is used to calculate the total losses in solid non-laminated materials, hence, hysteresis and anomalous losses are neglected in these parts. Consequently, calculated losses within these parts will give a low estimate. Neglecting the temperature dependency of conductivity further reduces the estimated losses.

Power loss neglected on the solid parts of the machine are hysteresis losses. These losses are found to be proportional to the area of the hysteresis curve and is defined as [9] [10]:

$$P = k_h B_{max}^2 f \tag{5}$$

In laminated parts of the machine, eddy currents are confined within each laminated sheet. The associated losses are given by:

$$P_c = \frac{\pi^2 \sigma d^2 B_{max}^2 f^2}{6} = k_c (B_{max} f)^2 \tag{6}$$

known as *classical losses* [11]. d is the lamination thickness, σ is the conductivity, B_{max} is the peak flux density of the sinusoidal flux in the material with corresponding frequency f. (6) is considered a gross simplification due to the neglecting of magnetic domains movement and a homogeneous magnetization in space. Therefore, a added term called *excess losses* is introduced to account for these effects. Analytical equations indicate that these are proportional to $(B\ f)^{3/2}$ [9]. Consequently, the third term for the core losses becomes:

$$P_e = k_e (B_{max} f)^{3/2} \tag{7}$$

The resulting core losses are the sum of (5 - 7), giving:

$$P = k_h B_{max}^2 f + k_c (B_{max} f)^2 + k_e (B_{max} f)^{3/2} \tag{8}$$

Coefficient k_c is given by (6), rendering (8) to a set of equations with two unknowns, k_h and k_e. They are found using core loss measurements. Measurements at several frequencies and flux densities gives the best fit. Different values of k_h and k_e are computed depending on the measurements used. A negative value of k_e gave the least error. This has no physical interpretation, hence, the last term in (8) is neglected. The best fit values in (8) with zero k_e gives a correlation with the measured results seen in Fig. 4. Note that at higher frequency the error between the measured and calculated core loss becomes larger.

Another source of error regarding core losses using these values are the non-sinusoidal shape of the flux densities. (8) assumes single frequency flux density. Machines with large amount of harmonics may not adhere to (8), introducing a new error in the calculations. Methods to correct for the distorted flux densities are given in [12] and [13] where correcting factors to the terms in (8) are introduced. The correction coefficient is calculated on the basis of a Fourier series expansion of the flux density. Since no measurements of the distorted flux density waveform is available, these factors are not introduced in the core loss computation. However, the knowledge of increased losses due to harmonics in the flux density indicate a higher core loss value than computed.

D. Flux Barriers

Flux barriers indirectly affect the harmonic content of the machine, contrary to the winding layout directly being the source. Flux barriers are structures with low reluctance, placed in the magnetic circuit of the machine, such as the rotor and stator yokes. The structures could either be air-gaps, cut-away parts, thinner yokes or materials with lower permeability than those of the stator or rotor yoke. Anisotropic material could also be

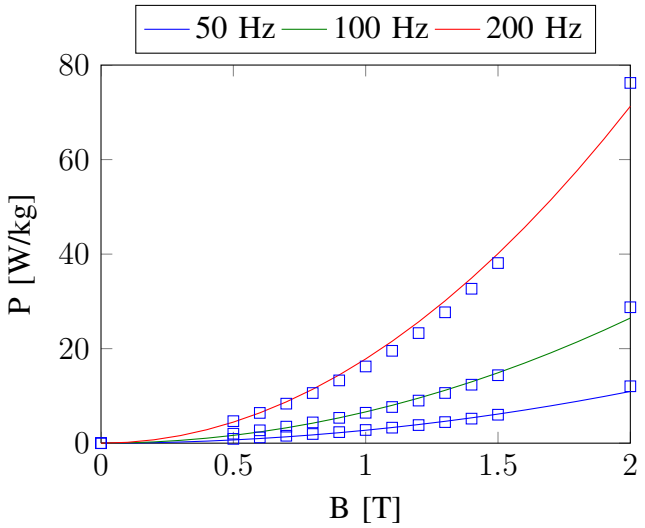

Fig. 4. The comparison of measured values for 50,100 and 200 Hz with the approximation to (8), neglecting the last term. Blue squares are measured values. This is the best found fit. The coefficeints $k_e = 337.35$.

used with the correct design. By introducing flux barriers the magnetic circuit changes and the flux through the barrier is reduced or forced to flow in a different path.

Correct placement of the flux barriers only affects the sub-harmonic flux, leaving the main harmonic flux to flow in the appropriate path. Note that the structural integrity of the machine must be contained, and as such, limits to the location of flux barriers may occur. Flux barriers might add ripple torque if the amplitude of the main harmonic changes during operation, and consequently, the right design of flux barriers is important in certain applications.

Flux lines produced by the single layer winding, without magnet excitation, are seen in Fig. 25. Particularly noticeable are the fundamental harmonic flux spanning 24 slot pitches. Introducing a flux barrier in the path of the fundamental harmonic flux reduces the amplitude and thereby reduces the losses associated with this harmonic.

[5] introduces 2 mm tangential air-gaps in various parts of the machine, including the stator, under each magnet and also a thinner rotor yoke, for a single layer 36 slot, 34 pole machine. Results indicated a 6 + 6 sectioning of the stator gave the highest reduction in Total Harmonic Distortion (THD). However, air gaps in between and under each magnet also showed promising results. Torque ripple in the 6 + 6 sectioning was stated as a concern and are not fully investigated, yet dividing the rotor under each magnet is believed to be most favourable regarding magnet flux and ripple torque. Another variation suggested by [5] and [14] would be to construct the stator by modular E-shaped cores where each E-section and coil would have a flux barrier adjacent to the next section. [4] presents a 12 slot 10 pole machines with flux barriers in the stator where different variations to the realisation of the flux barrier are presented regarding cooling channels and increased slot depth.

E. Genetic Algorithms

Genetic algorithms (GA) are a mathematical optimization tool inspired from evolutionary theory and hereditary. GA mimics the process of natural selection using a population of individuals were the best individuals are chosen to populate the next generation using crossover and mutation operators. A single individual in the population is described by its genotype and phenotype, respectively, the type of genes the individual is carrying, and how these genes come into appearance displaying certain attributes.

For a selection process to occur the best fit individuals in the population must be determined. A fitness function evaluates the phenotype with respect to the wanted attributes, consequently, each individual is characterized by a scalar fitness value describing its performance. The best found individuals are selected for crossover, were the genes of each individual are mixed with another fit individual, passing the best genes to the next generation. Over several generations the genes giving the best attributes are contained within the population and the algorithm has converged to a optimal solution.

The success of finding a global optimum in a short period of time, with the least computational effort is the selection of proper chromosome representation, crossover and mutation operators [1].

1) Fitness function: The fitness function maps the chromosome string, the genotype, into the phenotype and evaluates the fitness of each individual, based on the wanted attributes. A entry in the chromosome string represent the number of turns of a coil, or the existence of flux barrier in the machine. Mathematical operations such as Fourier series or FEA maps the chromosome string into its

phenotype giving the attributes:

$$y = f(x) \tag{9}$$

were f is the Fourier series calculations or the FEA, x is the chromosome string and y is the harmonic spectrum used in evaluating the fitness value. Several *partial fitness values* can compose the final fitness value, for instance the harmonics below the main harmonic are unwanted giving a high partial fitness value. Were as the main harmonic is evaluated as a separate partial fitness value. Consequently, the weighted sum of the partial values gives the final fitness value and the probability for the individual becoming a parent to the next generation.

2) Fitness scaling: The fitness value of a individual can range from e.g. 100 to 0.1, this gives a large difference in probability for a individual to be chosen. Therefore the fitness values are scaled according to $1/\sqrt{n}$, were n is the rank of each individual in the generation. Thus reducing the difference in probability, reducing the likelihood of fit individuals taking over the gene pool. Ensuring a large search space and avoiding convergence to a local minima [15].

3) Roulette wheel selection: Roulette wheel selection is the selection of parents to the next generation. With the probability assigned from the fitness scaling function, a random selection is performed were more fit individual has a larger chance of being selected.

A option to roulette wheel is tournament selection where randomly small groups are selected to compete against each other. This reduces the need for sorting individuals based on their fitness, giving a shorter computing time for large populations [16].

Crossover fraction gives the populations percentage selected for crossover operations, the remaining individuals are selected for mutation operation.

4) Crossover operators: Crossover operators generate offspring populating the next generation, ensuring convergence. Two parents, selected by the roulette wheel function, swap genes forming a new individual. Exchanging genes are performed in several ways, one point crossover where one random index point in the chromosome string split the genes. Two point crossover with two index points splitting the genes. Scattered crossover were a random generated mask maps the genes from each parent into the offspring.

In constrained problems the above operators may create offspring violating the constraints, as a consequence, custom operators always creating feasible solutions may be applied.

5) Mutation operators: Individuals not selected for crossover are selected for mutation. This operator introduces a small change in the population, providing genetic diversity and extending the search space. Gaussian mutation adds a random number from the Gaussian distribution to the chromosome string. And decreases the standard deviation as a function of generation count [15]. Consequently, decreasing the search space and allowing convergence. The next generation is formed by the union of crossover and mutation children, discarding the previous generation and performs a new fitness evaluation. The algorithm terminates when no change in average fitness occurs and the algorithm has converged to a solution.

Other operators such as elite individuals could be introduced, were the best fit individual is directly passed to the next generation without mutation and crossover operations. Ensuring the best individual is preserved and the best genes are always in the gene pool. Although convergence to a local minima can occur.

III. Method and Models

A. Winding layout GA

1) Partial fitness Functions: Multiple partial fitness values are used in describing the total fitness of each individual [3].

The first objective is the harmonics below the main harmonic:

$$Z_1 = \sum_{n=1}^{n=p-1} (F_n/F_p)^2 \tag{10}$$

where p is the main harmonic order, equal to the pole pair number. And F is the harmonic amplitude. The second objective concerns harmonics adjacent to the main harmonic:

$$Z_2 = \frac{F_p \cdot F_{p\pm1}}{1/4(F_p + F_{p\pm1})^2} \tag{11}$$

A third objective is the weighted sum of the harmonics:

$$Z_3 = \sum_{n=1}^{n=k} \left(\frac{F_n/F_p}{n-p} \right)^2 \tag{12}$$

where all harmonic up to order k are summed.
The fourth objective function is connected to the main harmonic winding factor ζ:

$$Z_4 = (1 - \zeta)^2 \tag{13}$$

In the flux barrier algorithm, the fitness function used are the weighted sum of the harmonics below the main harmonic, with the fundamental harmonic weighted the most.

$$Z_5 = \sum_{n=1}^{n=p-1} \left(\frac{F_n / F_p}{n} \right)^2 \tag{14}$$

2) Double layer GA: This algorithm uses Matlab global optimization toolbox, but with custom crossover and mutation operators in order to obey the constrains. Consequently, not needing repair algorithms. The chromosome vector is constructed of 8+8 floating point entries. A gene, a pair of two values, are the *index number* + 8. E.g. index one and 9 form a gene describing one coil of phase A. The first 8 entries describe the tooth number where each coil is placed. That is, an integer from 1 to $Q = 24$. A zero value indicate no coil. The next 8 entries describe the fractional number of turns and direction of each coil. E.g index 5 and 13 with values 2 and -50, is translated into 50 turns, clockwise wound around tooth 2. The number of turns are not the true number of turns since the number of turns is scaled to obtain the correct A-turns and torque. Dividing the chromosome vector up into two parts allow for easier use of crossover and mutation operators.
Performing crossover or mutation operations the two layer winding constraint must be satisfied. The chromosome vector describes coils of phase A, consequently the other phases placement are shifted $\pm 2\pi/3$ electrical radians, occupying another tooth. When crossover or mutation operation is performed, a table of available teeth's are used in choosing the next coil placement.
In certain cases crossover between two individuals cannot swap all the genes due to the constraints. This is solved by assigning a random gene, not found in any of the parents, to create a complete individual. This introduces an increase in the gene pool and may cause the algorithm to converge slower than it otherwise would. Code for these functions is found in the Appendix.

3) Four layer GA: In the four layer winding GA, no constraints on the problem is applied. Thus using standard crossover and mutation operators valid individuals are always created. The chromosome vector is of length $Q = 24$, with floating point values, were the index describe the tooth number, and the value describe the number of turns and direction of the coil. For example, index 8 in the vector has a value -30. This is translated into the coil, belonging to phase A, on tooth 8 has 30 fractional turns, wound in the clockwise direction. Consequently the other phases would have the equal number of turns on another tooth $\pm 2\pi/3$ electrical radians shifted away.

B. Machine / FEA model

The machine investigated is a 24 slot 22 pole, inside out rotor. Application of armature excitation for multiple layer winding is idealized, and a realized machine may have coils shape another way. Nevertheless, the error in the model is small regarding coil modelling, not taking eddy currents and skin effect into account. The physical constraints on the coils are are outside the scope of this report.
Transient simulation is performed with a step time of 2 ms to accurately model the harmonics with high time constants. With 2D modelling, end-effects are neglected and the model assumes induced currents can circulate the complete machine. Consequently electrical insulation between conducting parts is not taken into account. This introduces a error regarding the accuracy of the loss calculations.
Eddy currents are only induced in the non-laminated parts, including rotor yoke, magnets and solid stator ring. Within these parts core losses such as hysteresis and anomalous losses are not modelled due to lack of data. The laminated stator yoke accounts for such losses. Nominal speed of the rotor are 71 rpm with a applied frequency of 13 Hz. Other operation speeds where not considered.
Air-gap flux density plots are calculated in the middle of the air gap, reducing the effect slotting have on the flux distribution.

C. GA-FEA connection optimizing Flux Barriers

Single layer winding showed the highest amount of sub harmonics, hence this was the choice of winding layout in the optimization. Optimizing the flux barriers width and placement using GA and

FEA uses the two software packages, Matlab Global optimization toolbox and Ansys Maxwell. Ansys Maxwell includes a GA optimization tool, however, it does not allow using the air gap flux density harmonic spectrum as a fitness function. Matlab is therefore used as the main program, controlling the execution of the algorithm, creating the population and performing crossover and mutation operations. Secondly, a Visual Basic script interfaces Matlab with Ansys Maxwell creating the wanted geometry, and executes the FEA. Thirdly, Ansys Maxwell writes a file containing the air-gap flux density harmonic spectrum, lastly, being read by Matlab and evaluated in the fitness function. The fitness function used are the weighted sum of all harmonics below the working harmonic, (14).

Flux barriers, with relative permeability of one, where implemented with varying width of 0,7,14,21 mm beneath each slot and in the middle of each tooth, illustrated in Fig. 41.

The problem formulation has 2x24 variables, each variable taking 4 values. Binary chromosome vector are preferred due to the fixed number of values in each flux barrier, giving a 2 bit gene of ones and zeros translated into the width of each flux barrier. Resulting in a 96 bit long chromosome string.

Due to the area of the solution space and computation time the width of each flux barrier were set to only 0 or 14 mm, making the algorithm more prone to finding the global optimum in a reasonable time aspect.

Stationary FEA at one instant of time, without magnet excitation were used to calculate the air-gap flux density.

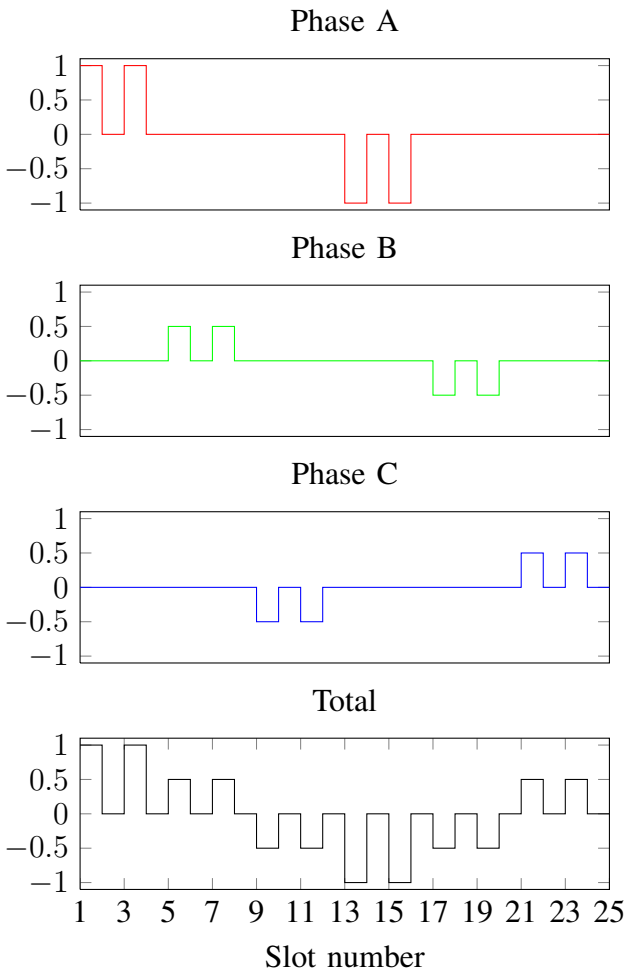

Fig. 6. Magnetomotive force (MMF) produce by single layer.

D. GA-MEC connection optimizing Flux Barriers

Following the failure of GA-FEM a Magnetic Equivalent Circuit (MEC) where implemented to optimizing the placement and width of the flux barriers. A MEC with linear permeability gives a linear set of algebraic equations, and reduces computation time compared to FEA. Correct valued flux densities are not acquired, but are neither the goal. MEC is used as a approximation, and the difference in flux densities between the different variations are of interest.

Due to the reduced computation time another third set of flux barrier in the rotor yoke where introduced, and as in GA-FEA each flux barrier could take the width of 0,7,14,21 mm.

Permeability of iron structures are high compared to the air gap and flux barriers, thus reluctance of iron parts were neglected to simplify the calculations.

The optimization problem has 3x24 variables giving a binary chromosome string of length 144, each gene is a pair of two bits describing the width of a flux barrier. The partial fitness values used are (14), evaluating the weighted sum of all harmonics below the working harmonic.

To ensure a symmetric flux-path in time, the current applied where taken at three instances of time, $\omega t = 0,\ 2\pi/3,\ 4\pi/3$. The harmonic spectrum where calculated at each instant of time and the difference in the main harmonic at the three instances where used as a partial fitness value.

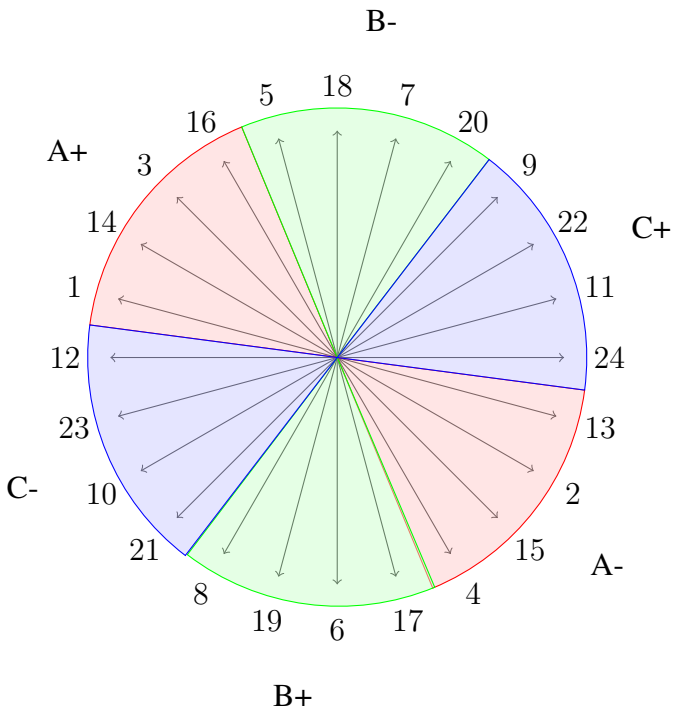

Fig. 7. Star of slot, $\pi/3$ rad sectors. Used in finding the single and double layer winding layout.

IV. Results: Winding Layout

A. One layer winding

The simplest winding layout for a Concentrated Coil (CC) permanent magnet (PM) machine are the single layer winding. This choice gives a easy manufacturing and assembly process since the compact coils can be pre-fabricated and slides directly into the slots. There is neither any overlap between phases, in the slots or the end windings, giving a fault tolerant machine. Using the star of slots the highest winding factor for the main harmonic can be made. Fig. 7 displays the star of slot with $\pi/3$ phase spread. This produces a winding layout as seen in the linear stator in Fig. 5, where dot marks positive current direction out of the plane, and cross marks current into the plane. Slot number one is the first slot from the left and increases towards the right. Visualisation of the end coils are seen in Fig. 8 and as noted no end winding overlaps.
The idealized Magnetomotive Force (MMF) produced by the single layer winding layout are seen in Fig. 6 with current applied at time $t = 0$ with the following symmetrical currents:

$$i_a = \hat{I}\cos(\omega t)$$
$$i_b = \hat{I}\cos(\omega t - 2\pi/3)$$
$$i_c = \hat{I}\cos(\omega t + 2\pi/3)$$

Where $\hat{I} = 1$ pu.
The idealized mutual inductance is zero due to the zero valued MMF at the position of the other slots than the phase in question.
The normalized harmonic spectrum generated by this winding layout is seen in Fig. 22. As noted high amount of sub-harmonic spatial fields are present in the machine. In fact the fundamental harmonic is of lager amplitude than the main harmonic. Other harmonics of considerably magnitude involved are the 5.th,7.th,13.th.
The winding factor for this winding layout is seen in Table I.

layer	k_w
1	0.9577
2	0.9495
4	0.9248
GA 2	0.9535
GA 4	0.906

TABLE I
Winding factor for different winding layouts. GA 2 are the two layer produced by the GA. GA 4 are the four layer produced by the GA

B. Two Layer winding

A two layer winding can be made with the use of the star of slots in Fig. 7, using the phasors twice since. The two layer layout is illustrated in in Fig. 13, with end coils visualized in Fig. 14. This winding layout has coils from different phase in the same slot, increasing the risk of phase to phase short circuit. The MMF produced by this winding layout is depicted in Fig. 9. Noticing that each tooth now contain a coil, forming a more pronounced return path for the flux in a adjacent tooth.
The normalized spectrum of the total MMF is plotted in Fig. 22. A substantially increase in the main harmonic is observed, and a decrease in fundamental harmonic is achieved. The winding factor has decreased due to the change in distribution factor as seen in Table I.

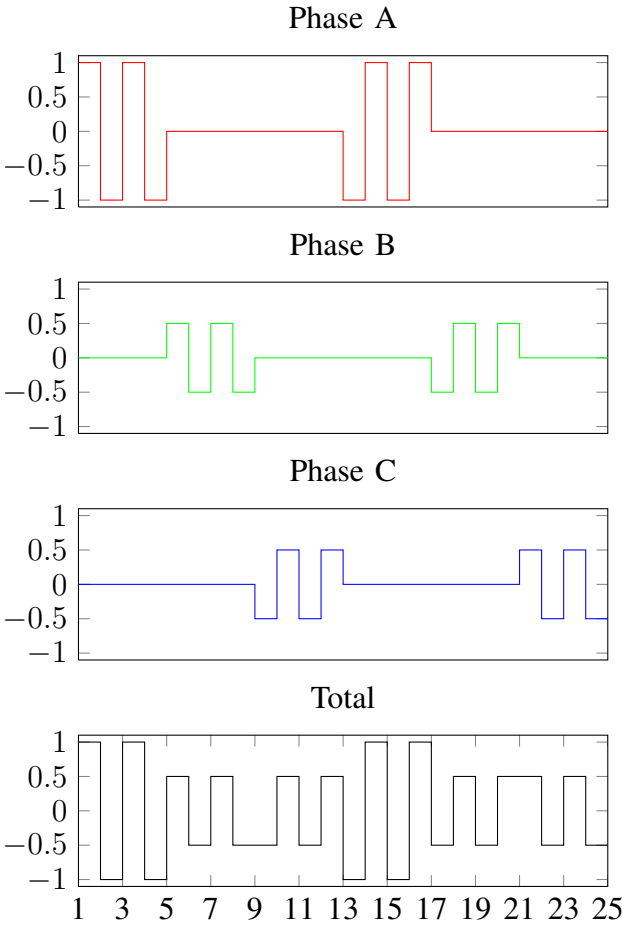

Fig. 9. Magnetomotive force (MMF) produce by double layer.

C. Four layer winding

Increasing the number of layers to four further manipulation of the MMF in order to increase the winding factor, or decrease the spatial harmonics is performed. Doubling the sector in the star of slots as seen in Fig. 10 and shifting the outer sector by a angle $\alpha_{sh} = 15°$, equal to the angle between two adjacent phasors [17], gives the winding layout seen in Fig. 15 and Fig. 16. As noted this produces a three layer winding, and not all of the available space in the third layer is used. The corresponding MMF produced by this winding is seen in Fig. 11. Noticing from the MMF plot and the end coil figure that some teeth's contain two phase windings, consequently increasing the mutual inductance, making this a solution less fault tolerant. Fig. 11 corresponding spectrum is seen in Fig. 22. As noticed the main harmonic is increased w.r.t. the two other layers, the 1.th and 5.th harmonic are still present.
Fig. 22 shows the normalized values of the harmonic

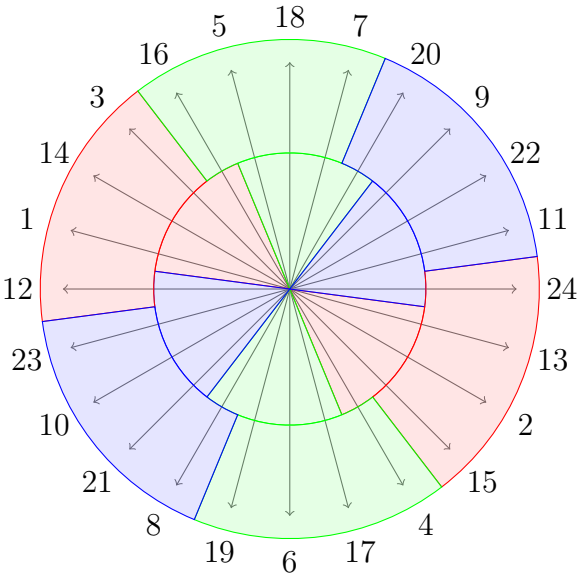

Fig. 10. Star of slot used in the four layer winding layout. Used in finding winding layout for the four layer winding.

spectrum. Noticing the fundamental harmonic is reduced with the two and four layer winding. The reduced winding factor is seen in Table I.

D. Four layer version 2

Due to the available space in the four layer winding, filling the space with the appropriate phase winding can present a better solution. Optimizing the layout with respect to the winding factor results in the MMF seen in Fig. 12, along with the harmonic spectrum in Fig.22. As noticed this solution gives a rise in the fundamental harmonic compared to the ordinary four layer winding making it a less attractive choice.

E. Genetic Algorithm Double Layer winding

With the parameters in Table II, the same parameters used in [3], the GA with double layer constraints converged to the solution with fitness value of 0.8125. And a chromosome vector:

$$7, 7, 5, 1, 7, 5, 19, 18, 19, 20, 8, 18, 17, 8, 6, 20, 6,$$
$$0.934, 0.778, 0.618, -0.700, 0.745, -0.791, 0.959$$
$$, -0.857, 0.605, -0.510, 0.614, -0.593, -0.653$$
$$, -0.836, 0.554, -0.618$$

Translated into the MMF seen in Fig. 21 with the corresponding spectrum in Fig. 22. The fundamental

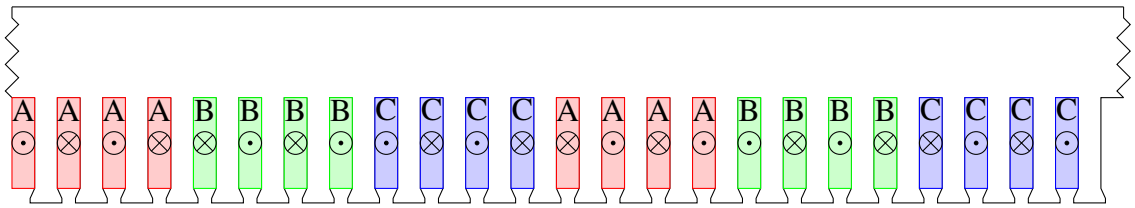

Fig. 5. Illustration of the single layer winding layout in the stator of the machine. Color red indicates phase A, green phase B and color blue phase C. Circle with dot or cross marks the direction of turns.

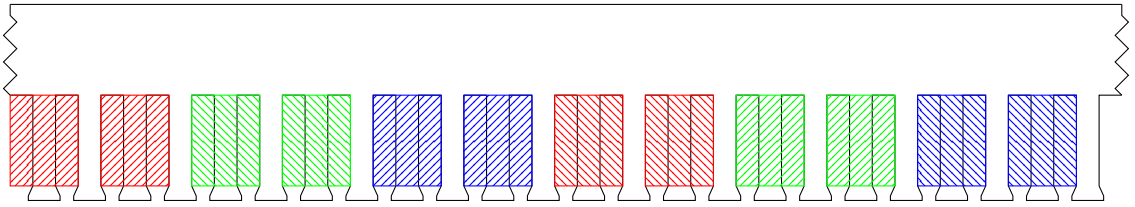

Fig. 8. Illustration of the single layer winding layout in the stator of the machine. Color red indicates phase A, green phase B and color blue phase C. Visualisation of end coils.

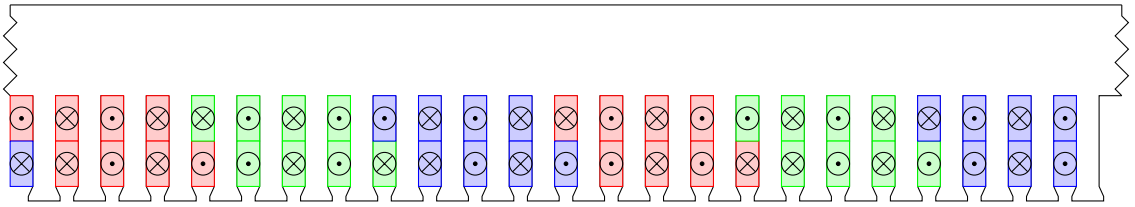

Fig. 13. Illustration of the double layer winding layout in the stator of the machine. Color red indicates phase A, green phase B and color blue phase C. Circle with dot or cross marks the direction of turns.

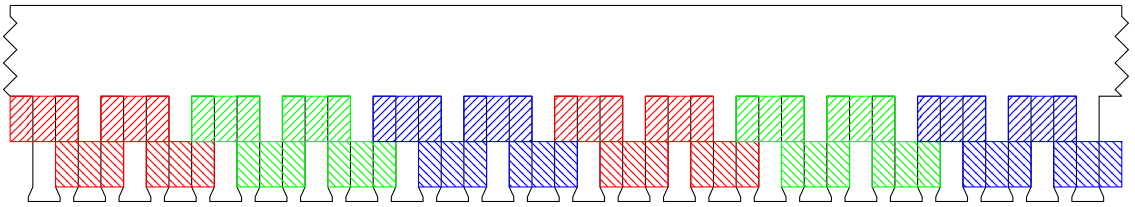

Fig. 14. Illustration of the double layer winding layout in the stator of the machine. Color red indicates phase A, green phase B and color blue phase C. Visualisation of end coils.

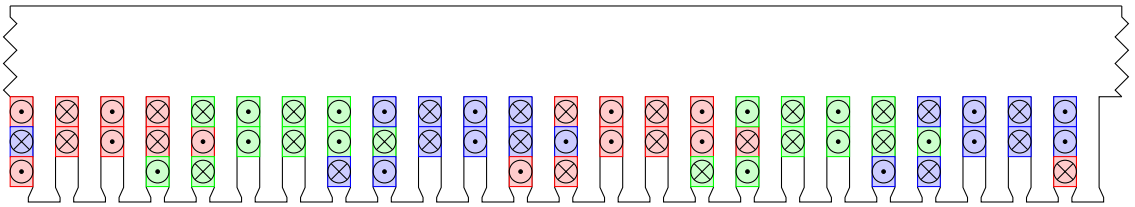

Fig. 15. Illustration of the four layer winding layout in the stator of the machine. Color red indicates phase A, green phase B and color blue phase C. Circle with dot or cross marks the direction of turns.

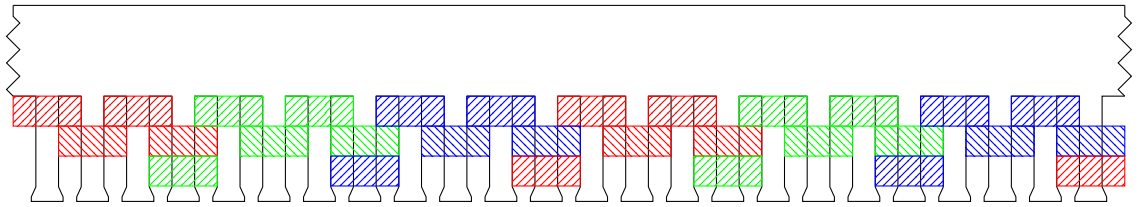

Fig. 16. Illustration of the four layer winding layout in the stator of the machine. Color red indicates phase A, green phase B and color blue phase C. Visualisation of end coils.

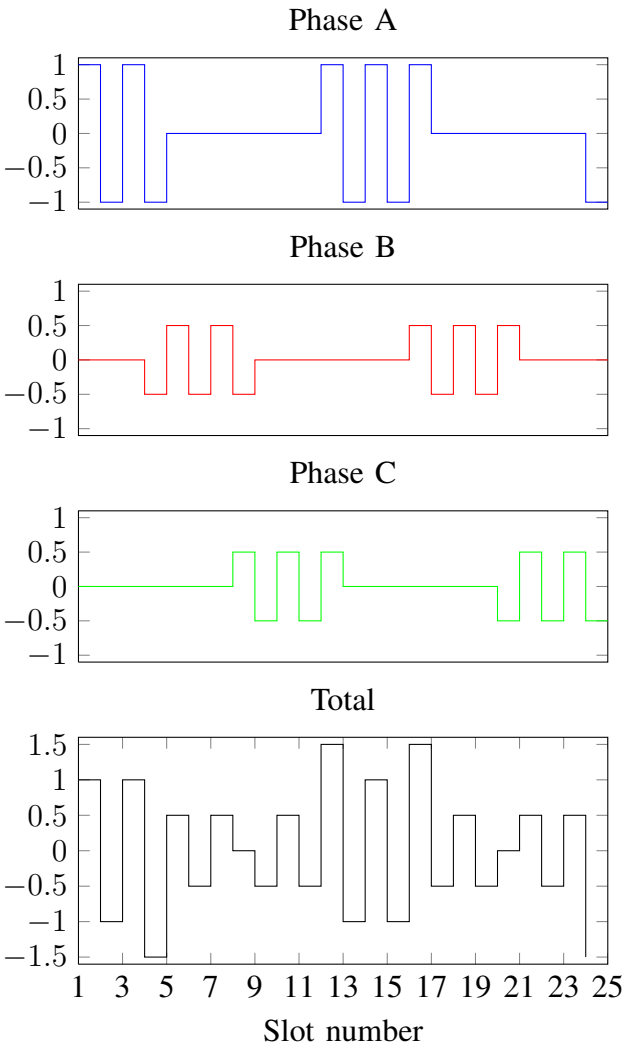

Fig. 11. Magnetomotive force (MMF) produce by four layer winding.

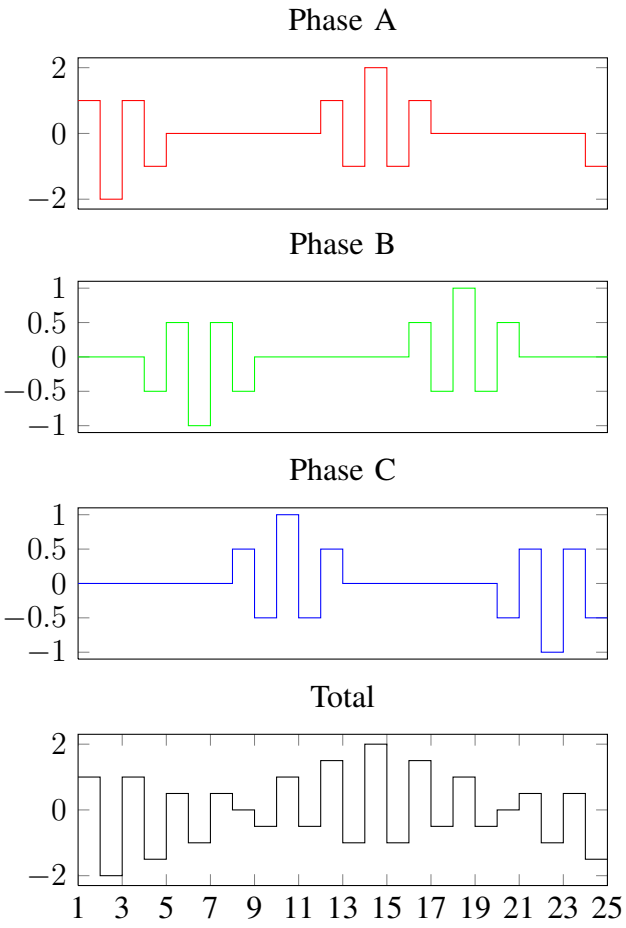

Fig. 12. Magnetomotive force (MMF) produce by four layer winding, version 2 with increased number of turns in certain slots

harmonic has decreased compared to the ordinary double layer, as has the 5.th harmonic. Contrary to the 7.th harmonic showing a increase. The winding factor is seen in Table I.

Fig. 17 illustrate the current direction of the coils in the slot. Positive current direction out of the plane is marked with a dot, were as positive current direction into the plane is marked with a cross. Fig 18 illustrate the number of turns on each coil. A wide end coil indicates more turns than the thin coils. Convergence statistics revealed a fitness value of 0.8843 in generation 283, and at generation 303 a individual with fitness value 0.8187, close to the final solution.

F. Genetic Algorithm Four Layer winding

The best found solution and convergence using the four layer GA used the parameters in Table

Population size	5000
Generations	3000
Crossover fcn.	custom
Crossover fraction	80%
Mutation operator	custom
Mutation fraction	20 %
Elite count	2
Evaluation count	$15005 \cdot 10^3$
Time used	~18 hours

TABLE II
PARAMETERS FOR FOR GA DOUBLE LAYER WINDING.

Population size	1000
Generations	3000
Crossover fcn.	scattered?
Crossover fraction	50%
Mutation operator	Gaussian
Mutation fraction	50 %
Elite count	0
Evaluation count	$3 \cdot 10^5$
Time used	~1 hours

TABLE III
PARAMETERS FOR GA FOUR LAYER WINDING.

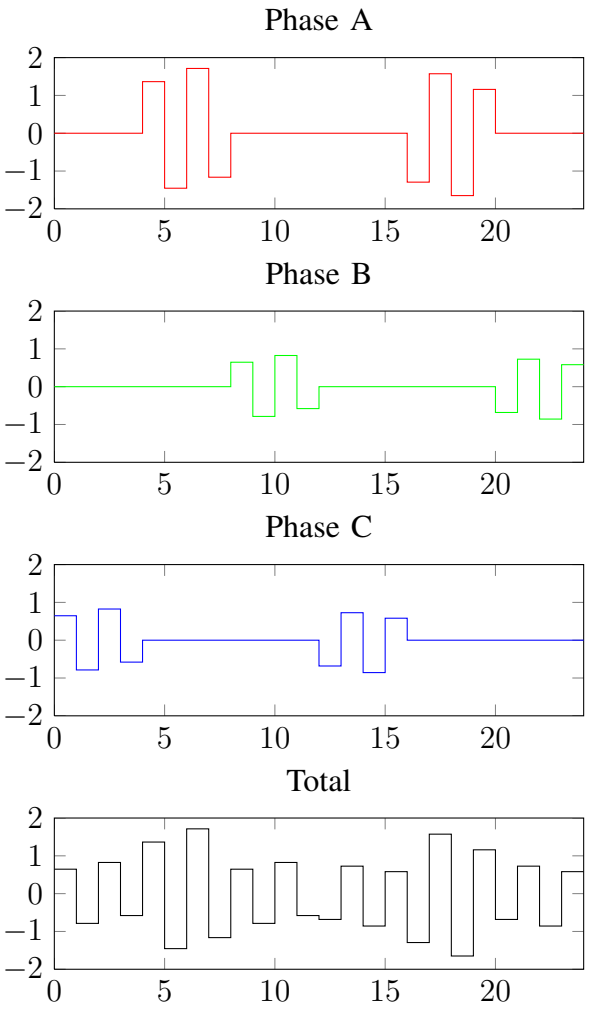

Fig. 21. Magnetomotive Force (MMF) produced by the GA double layer. Different turns on each coil produce a MMF of varying amplitude.

III. Giving the convergence plot seen in Fig. 23, illustrating the average distance in the population as a function of generations. The solution has a fitness value of 0.1880 with a chromosome vector:

$$0, 0, 0, 0, -44, 88, -126, 152, -124, 86, -42, 0, 0,$$
$$0, 0, 0, 44, -88, 127, -153, 124, -86, 42, 0$$

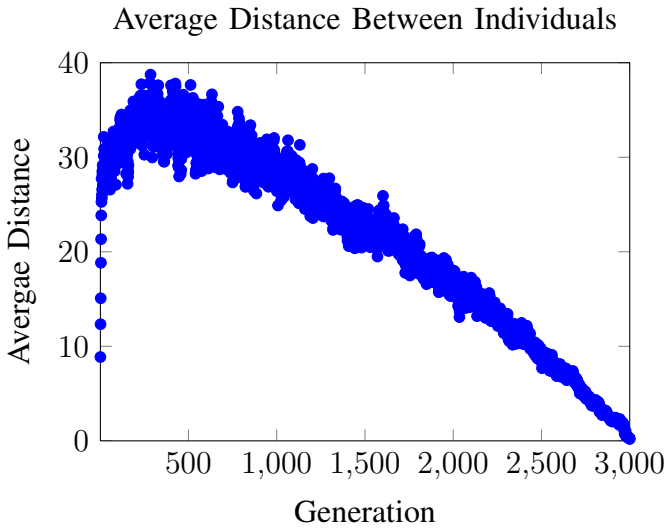

Fig. 23. The average distance within the population during the generations. The amount of mutation shrinks as the generation count increases. Little average distance at the end indicates the solution has converged to a optimum. High average distance ensures a good coverage of the solution space

giving the MMF plot in Fig. 24, with the corresponding harmonic spectrum in Fig. 22. As noticed all the sub harmonics are removed, as well some super-harmonics.
However a low winding factor is reported in Table I.
Fig. 19 indicates the current direction of each coil in the machine. Fig. 20 indicates the number of turns on each coil by increased thickness.

V. RESULTS FEA VERIFICATION

This chapter aims to present the results obtained from the FEA analysis of the different winding layout and the flux barrier solutions. The results presented are flux lines plots, with and without magnet excitation, air gap flux density plots from armature winding and the corresponding harmonic spectrum. Core and eddy current losses in stator, rotor and

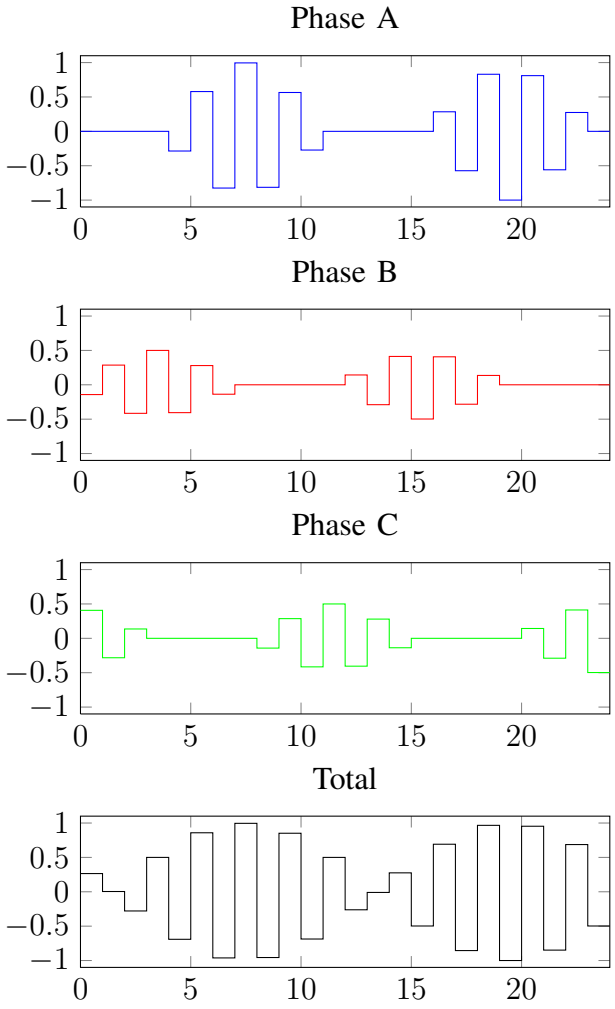

Fig. 24. Magnetomotive Force (MMF) produced by the GA four layer winding. Different turns on each coil varies the amplitude.

magnets are presented as well the inductances of the winding layouts. Each sub section is divided into a stationary analysis without magnet excitation, stationary analysis with magnet excitation and transient analysis.

A. Single Layer FEA

The single layer FEA is considered the benchmark in the following analysis due to the high presence of sub harmonics.

1) Without Magnet excitation: Neglecting the excitation from the magnets in order to quantify the flux produced by the armature winding gives the flux line plot seen in Fig. 25, along with the current density. Coulor red is phase A with 1 pu. current and blue is the other phases with -0.5 pu. current. Notice the path of the fundamental

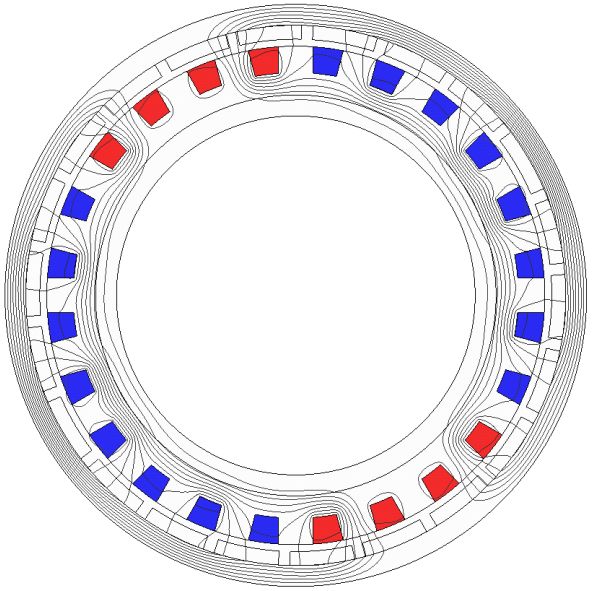

Fig. 25. Flux lines in the machine with single layer and without the excitation of the magnets, only armature excitation. Red; 1 pu current, Blue; -0.5 current

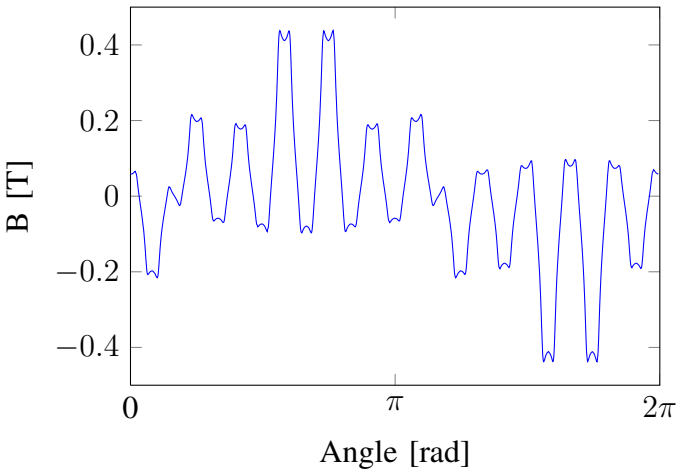

Fig. 26. Air gap flux density plot for single layer winding without magnet excitation. Horizontal axis equal to zero along the positive x axis in Fig. 25.

harmonic having a wavelength equal to 24 slots, where as the main harmonic has a wavelength equal to one pole pitch. The air gap flux density is seen in Fig. 26. Comparing with Fig. 6 one notices the similarities. The difference is a small non-zero flux in between the coils, along with the distortion in the flux due to slotting of the stator and air gap fringing.

The inductance matrix is seen in Table IV. As noticed, due to the harmonic content the flux linkage between the phases are different.

Taking the Discrete Fourier Transform (DFT) of the air gap flux density in Fig. 26 the harmonic spectrum in Fig. 31 is obtained. Comparing to Fig. 22 the analytical approach is verified.

2) With Magnet excitation: Applying magnet excitation the contribution from the magnet flux changes the flux distribution. Fig. 26 shows a peak value of 0.4 T in the air gap, were as the remanent flux density of the magnets are 1.2 T. Consequently, the magnet flux will govern the flux distribution. The flux lines along with the current density are seen in Fig. 27.

Fig. 28 shows the air gap flux density. As noticed the main harmonic is more apparent now, and the sub-harmonics are less noticeable.

3) Single layer transient simulation: Transient simulation where run for 800 ms to gain steady state with a time step of 2 ms. The results is presented in Table VI.

	A	B	C
A	16	0.86	0.86
B	0.86	16	-0.19
C	0.86	-0.19	16

TABLE IV
INDUCTANCE MATRIX FOR THE SINGLE LAYER WINDING. IN μH

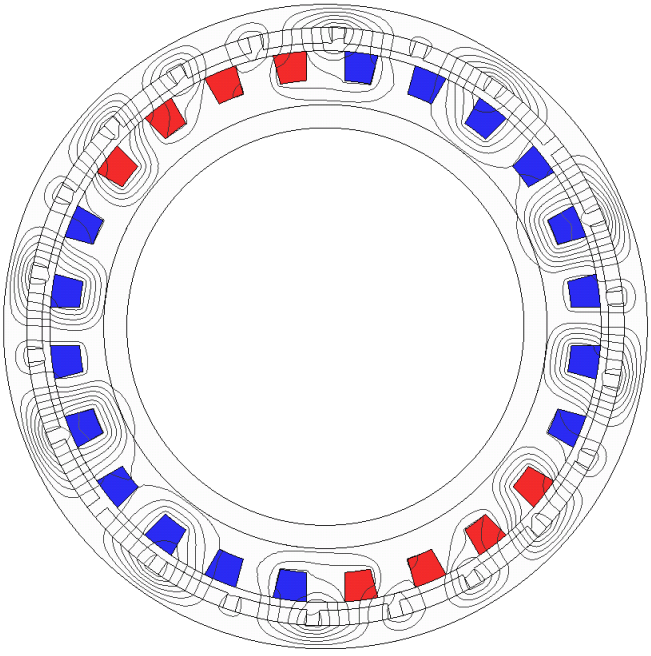

Fig. 27. Flux lines in the machine with single layer. With the excitation of the magnets and armature excitation. Red; 1 pu current density, Blue; -0.5 current density

B. Double Layer FEA

With the same current and number of turns the double layer winding layout produces a main harmonic with higher amplitude than the single layer. For a comparison on torque and losses the input current and number of turns are reduced for the double layer. The ampere turns for single layer where $\sqrt{2} \cdot 130$A 60 turns = 11030 A-turns, producing 7.3 kNm of torque at a speed of 71 rpm. $\sqrt{2} \cdot 65.8$A 60 turns = 5580 A-turns in the double layer produced the same output power.

1) Without Magnet excitation: Neglecting the excitation from the magnets the flux line plot of the double layer is seen in Fig. 29. Comparing with the single layer case in Fig. 25 the sub-harmonic flux are less distinct. Fig. 30 shows the air gap flux density with the corresponding harmonic spectrum in Fig. 31. As noticed the sub-harmonic are reduced. The inductance matrix is seen in Table V and as noted a small mutual inductance exists.

2) Double layer transient simulations: Transient simulation where run for 800 ms with a time step of 2 ms. The computed values are given in Table VI, and a reduction in losses is reported.

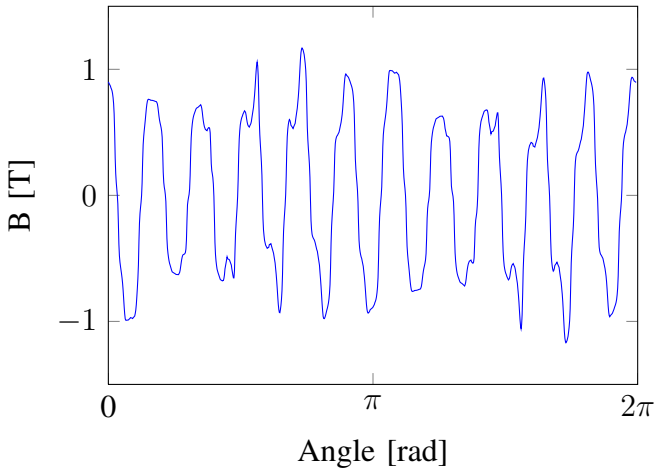

Fig. 28. Air gap flux density plot. With magnet excitation and armature excitation. Horizontal axis equal to zero along the positive x axis in Fig. 25.

	A	B	C
A	38.9	-0.72	-0.72
B	-0.72	38.8	-0.72
C	-0.72	-0.72	38.8

TABLE V
INDUCTANCE MATRIX FOR THE DOUBLE LAYER WINDING. IN μH

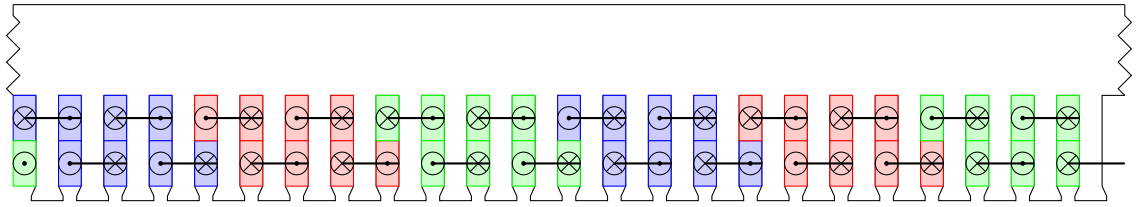

Fig. 17. Visualisation of current direction for the GA double layer winding. Red is phase A, Green is phase B, and Blue is phase C. Cross marks positive current direction into the plane into the plane. Dot marks positive current direction out of the plane

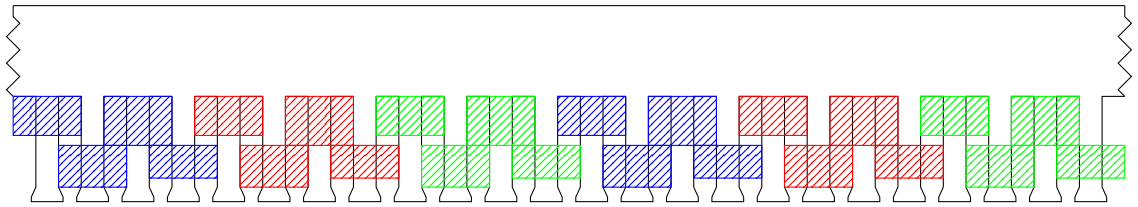

Fig. 18. Illustration of the double layer winding produced by the GA, layout in the stator of the machine. Colour red indicates phase A, green phase B and colour blue phase C. Visualisation of end coils

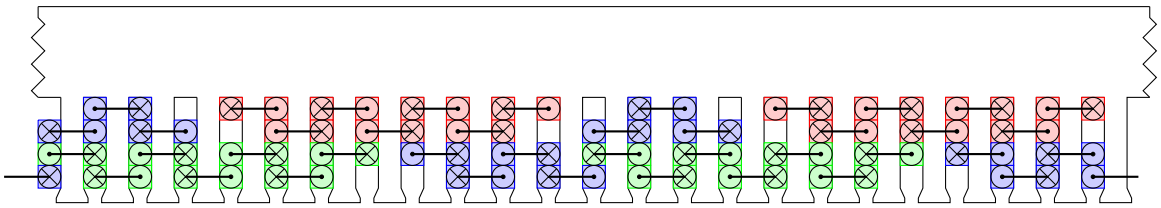

Fig. 19. Visualisation of current direction for the GA four layer winding. Red is phase A, Green is phase B, and Blue is phase C. Cross marks positive current direction into the plane into the plane. Dot marks positive current direction out of the plane

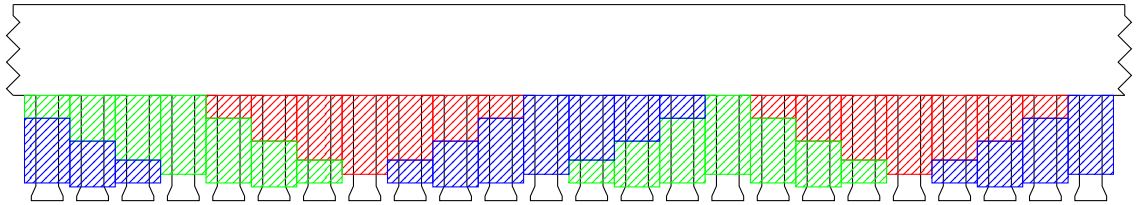

Fig. 20. Illustration of the four layer winding produced by the GA, layout in the stator of the machine. Colour red indicates phase A, green phase B and colour blue phase C. Visualisation of end coils. Thickness indicates dumber of turns of each coil.

	Single Layer	Double Layer	Four Layer	GA Double Layer	GA Four Layer	GA Flux Barrier
Torque [kNm]	7.4	7.38	7.44	7.22	7.47	6.2
Ripple Torque [kNm]	0.135	0.22	0.244	0.368	0.0657	0.774
Core Loss [W]	183	128.8	127.2	130	149	120
Magnet Loss [W]	1857	1234	1153.6	1253.5	981	1315
Rotor Loss [W]	2072	861.4	796	865.6	457	1207
Stator Ring [W]	0.5	0.4	0.4	0.43	0.42	-
Total Solid Losses[kW]	3.92	2.1	1.945	2.114	1.44	2.45

TABLE VI

RESULTS OBTAINED FROM TRANSIENT FEA SOLUTIONS. RIPPLE TORQUE IS PEAK TO PEAK.

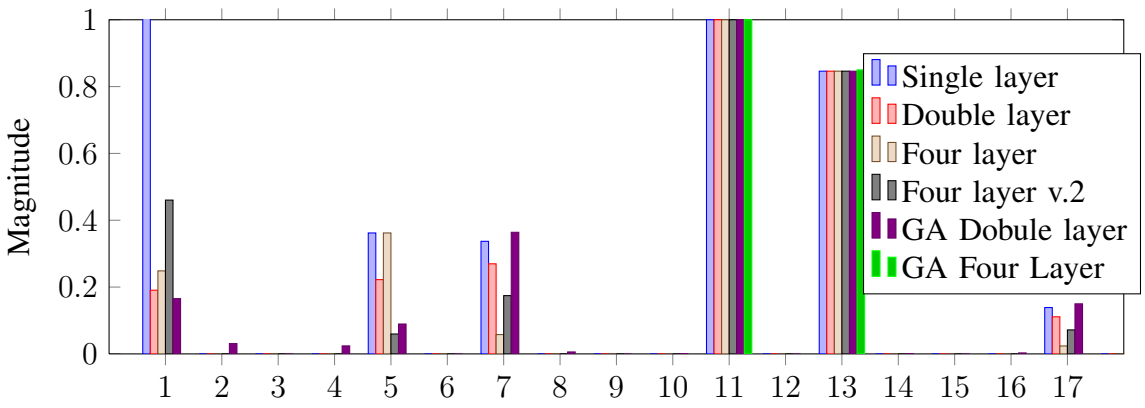

Fig. 22. Harmonic spectrum of the MMF for different winding solutions. Normalized w.r.t. the main harmonic. Idealized MMF case.

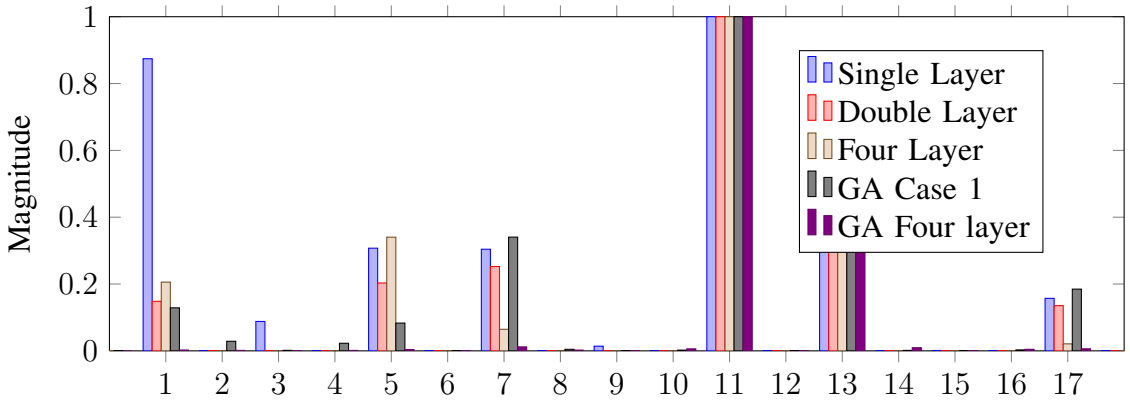

Fig. 31. Harmonic spectrum of air gap flux density obtained from FEA. Without magnet excitation.

	A	B	C
A	48.4	-9.9	-9.9
B	-9.9	48.3	-9.8
C	-9.9	-9.8	48.3

TABLE VII
INDUCTANCE MATRIX FOR THE FOUR LAYER WINDING. IN μH.

	A	B	C
A	39	-0.72	-0.72
B	-0.72	39	-0.72
C	-0.72	-0.72	39

TABLE VIII
INDUCTANCE MATRIX FOR THE GA DOUBLE LAYER. IN μH

C. Four Layer FEA

1) Without Magnet excitation: Flux plot with magnet excitation neglected is seen in Fig. 32. The air gap flux density are seen in Fig. 33 and the corresponding spectrum are seen in Fig. 31. The inductance matrix are seen in Table VII. As earlier suggested a mutual inductance between the phases exist due to the winding layout.

2) Four layer transient simulation: The transient behaviour of the four layer winding is investigated. Since it produces a higher main harmonic the phase current must be decreased to $I = \sqrt{2}\cdot$ 52.3 A 60 turns = 4440 A turns. Results are presented in Table VI.

D. GA Double Layer FEA

1) Stationary FEA: The flux plot without magnet excitation is seen in Fig. 34, along with the air gap flux density in Fig. 35. The corresponding spectrum is seen in Fig. 31, along with the inductance matrix seen in Table VIII.

2) Transient FEA: Results from the transient simulations are given in Table VI. The winding where made such that tooth with the highest number of turns had 100 turns, other coils had fractions of this number. Peak input current where $\sqrt{2}$ 46.5 = 65.8A.

As noticed the ripple torque are much higher for this winding layout, and no decrease in losses are

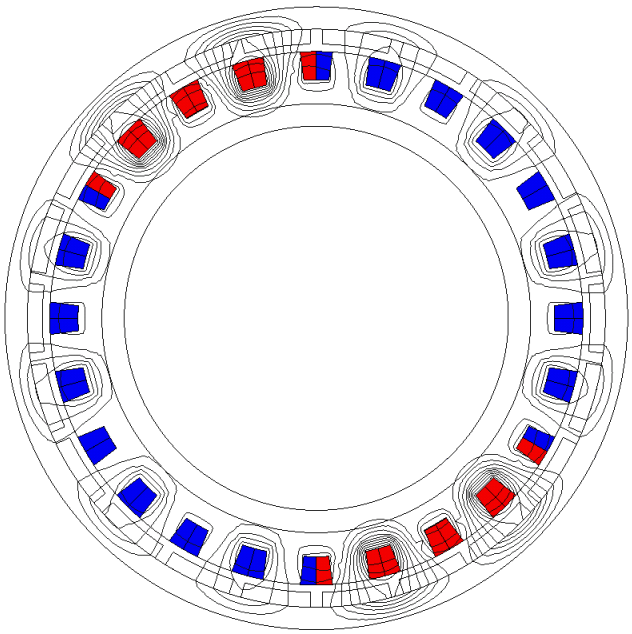

Fig. 29. Flux lines of the double layer winding. Without magnet excitation. Colors are current density in the coils, red are 1 pu, blue are -0.5 pu.

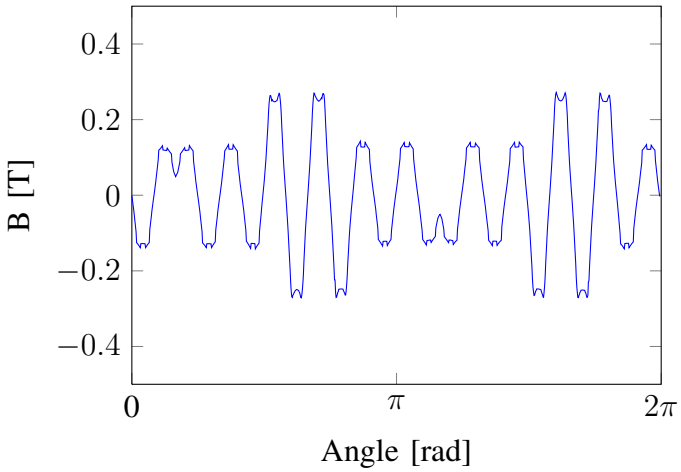

Fig. 30. Air gap flux density plot of the Double layer. Horizontal axis equal zero at the positive x axis in the plot.

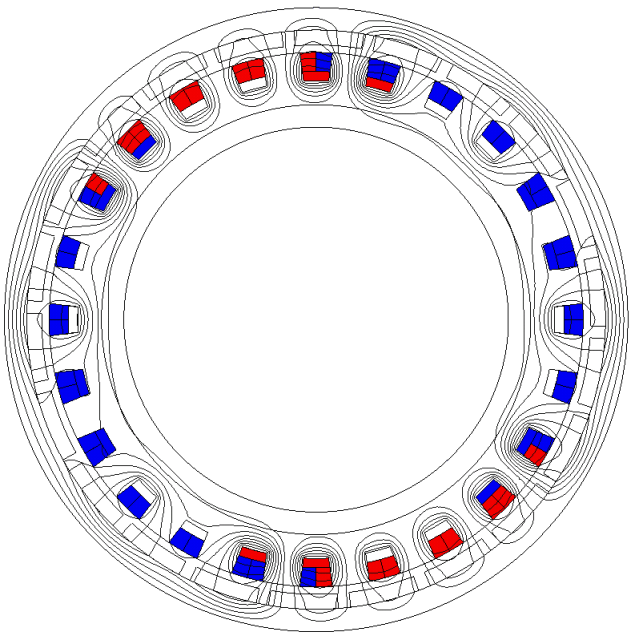

Fig. 32. Flux lines of the machine with four layer and without the excitation of the magnets, only armature excitation. Red; 1 pu current density, Blue; -0.5 current density

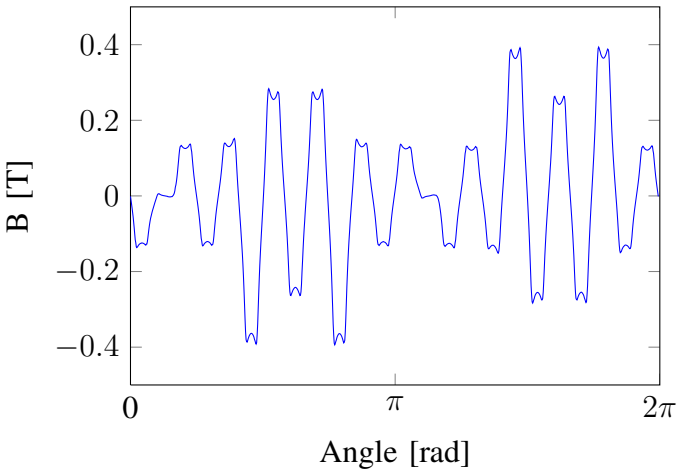

Fig. 33. Air gap flux density plot of the Four Layer. Without magnets excitation. Horizontal axis equal zero at the x axis in the plot.

reported.

E. GA Four Layer Winding

1) Without Magnet excitation: Neglecting the excitation from the magnets one observes the air gap flux density plot in Fig. 37 and the harmonic spectrum in Fig. 31. The flux lines plot are seen in Fig. 36. Turns on each winding are varying from 153 to 42, with a peak current of 72 A. The inductance matrix is seen in Fig IX, as noticed the mutual inductance is high.

2) Four Layer transient simulation: Transient simulation where performed over 500 ms with a time step of 5 ms. Results from the simulation are presented in Table VI. Notice the reduction in solid losses.

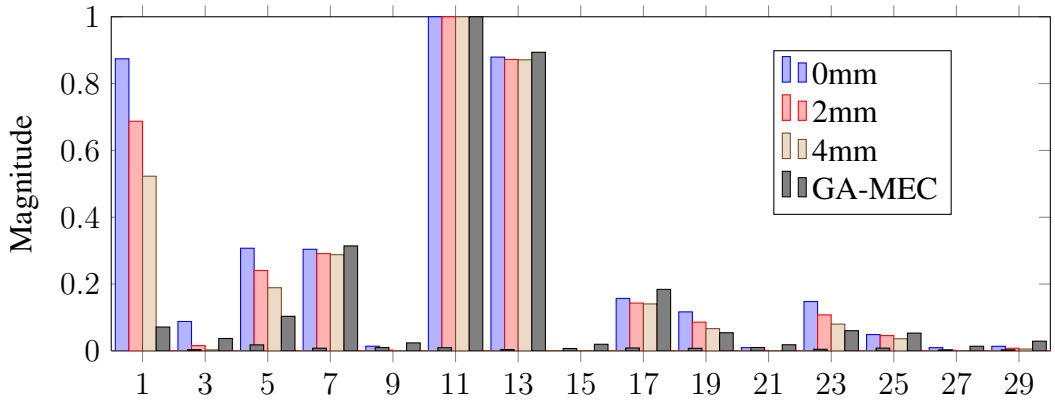

Fig. 40. Harmonic spectrum of air gap flux density in Fig.39 and Fig. 42, Single layer without magnets excitation. Different flux barrier configurations. Normalized values

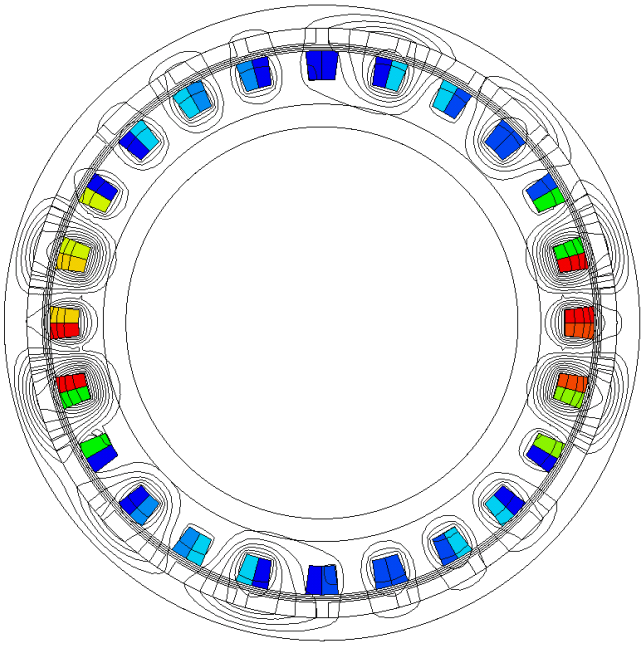

Fig. 34. Flux lines of the machine with GA Double Layer winding. Without magnets excitation, only armature excitation. Color indicate current density

	A	B	C
A	74.6	-27.8	-27.8
B	-27.8	74.5	-27.7
C	-27.8	-27.7	74.5

TABLE IX
INDUCTANCE MATRIX FOR THE NO MAGNETS CASE, GA FOUR LAYER. IN μH

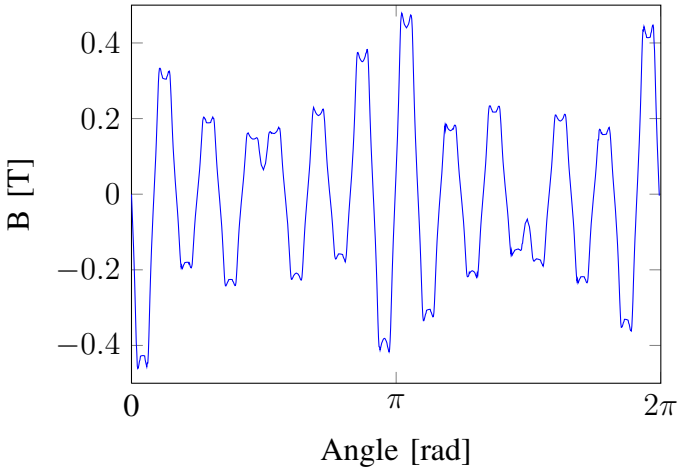

Fig. 35. Air gap flux density plot of the GA double layer. Horizontal axis equal zero at the positive x axis in Fig **??**GACase1FluxLines

	A	B	C
A	13.2	0.79	0.79
B	0.79	13.2	0.78
C	0.79	0.78	13.2

TABLE X
INDUCTANCE MATRIX FOR THE FLUX BARRIER CASE WITH 4 MM WIDTH. IN μH

F. 6+6 sectioning Single layer

As in [5] a 6+6 section of the stator where preformed since this was found to be the most promising solution. More specific, a flux barrier is placed under each slot adjacent to the next phase winding. The corresponding flux line plot is seen in Fig. 38, with a the air gap flux density is seen in Fig. 39 and the harmonic spectrum seen in Fig. 40. As noticed the flux barriers impact the fundamental harmonic, and has little impact on the main harmonic. From Fig. 38 it is noticed that flux penetrates into the non-laminated parts of the stator.

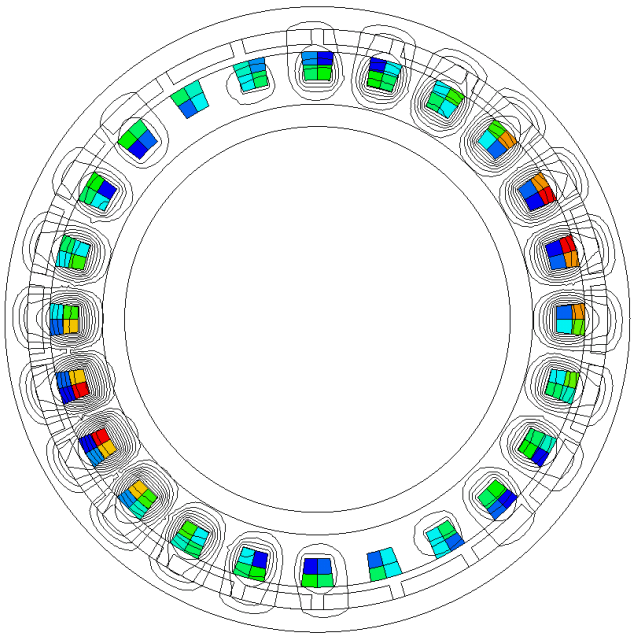

Fig. 36. Flux lines of the machine with GA Four layer winding. Without the excitation of the magnets, only armature excitation. Color indicate current density

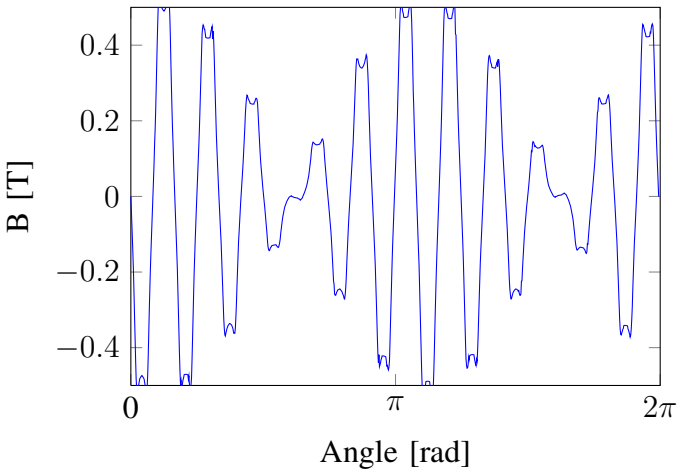

Fig. 37. Air gap flux density plot GA Four layer winding. Horizontal axis equal zero at the x axis in the plot.

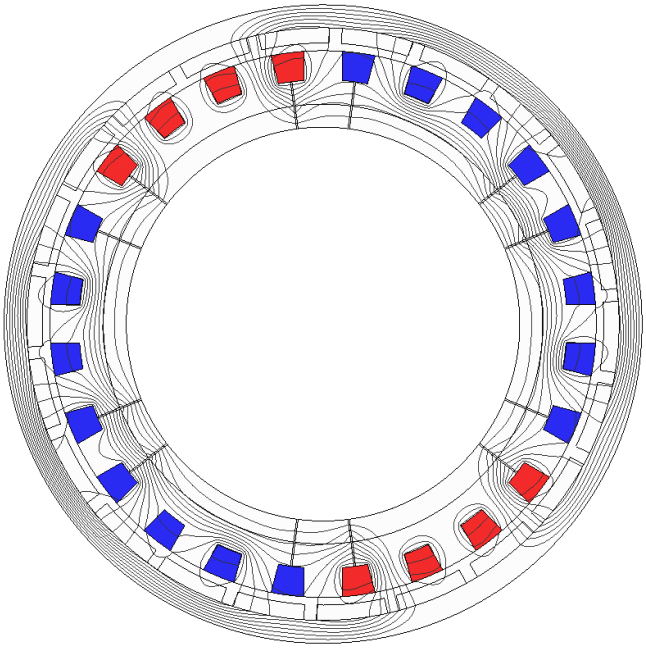

Fig. 38. Flux lines of the machine with single layer winding and flux barriers in the stator 6+6 sectioning. Without the excitation of the magnets, only armature excitation. Red; 1 pu current density, Blue; -0.5 current density. 6+6 sectioning of the machine

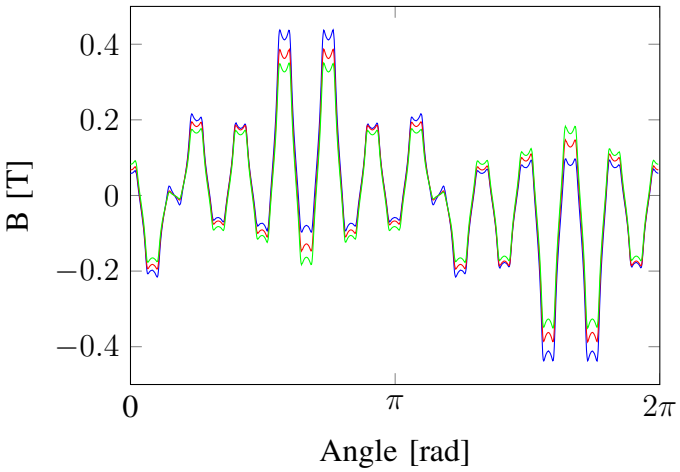

Fig. 39. Air gap flux density plot of different flux barrier widths. Horizontal axis equal zero at the x axis in the plot. 0mm blue, 2 mm red, 4 mm green

G. GA-FEM Flux Barriers

A GA optimization interconnected with the FEA where performed. The parameters used are seen in Table XI. After 10 generations the fitness value of the best individual where 0.1642, with the chromosome vector:

$$x = 0, 0, 1, 1, 1, 0, 0, 0, 1, 0, 0, 0, 0 \\ , 1, 0, 0, 0, 0, 0, 0, 0, 0, 0, 1$$

Giving a solution seen in Fig. 41. As noticed the sub-harmonic flux at time equal to zero is well suppressed, but at time equal to $2\pi/3$ rad the sub-harmonics are not suppressed. Thus the lack of symmetry in the solution will cause the sub-harmonic to varying in amplitude during operation. The main harmonic will also have a change in flux density amplitude causing ripple torque.

Population size	25
Generations	10
Crossover fcn.	scattered
Crossover fraction	50%
Mutation operator	Gaussian
Mutation fraction	50 %
Elite count	0
Evaluation count	250
Time used	4 hours

TABLE XI
INPUT DATA FOR GA-FEA FOR FLUX BARRIERS

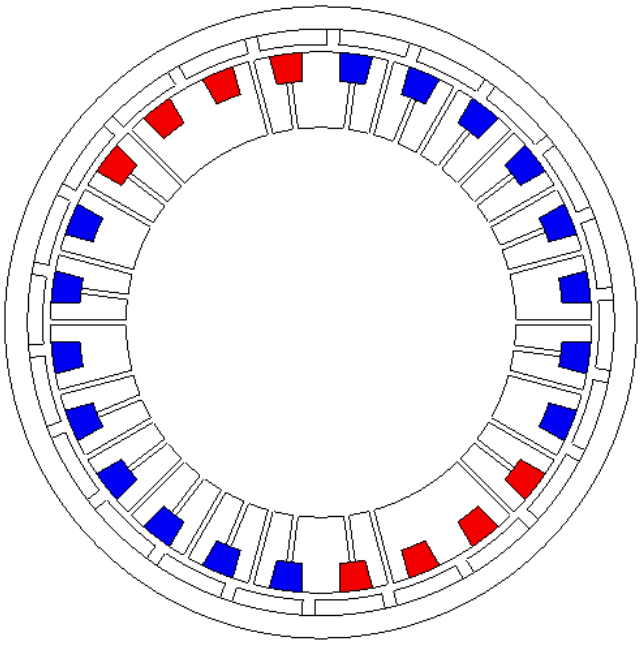

Fig. 41. GA-FEA solution. Width of air gaps are 7 mm. Single layer winding. Colors are current, red 1.0 pu, blue -0.5 pu.

H. GA-MEC Flux Barriers

Parameters used in the GA are seen in Table XII. The algorithm converged on a solution having a fitness value equal to -1.6872, and is illustrated in Fig. 42. As noticed the maximum width of the flux barriers were found to give the best results. Fig. 43

Population size	5000
Generations	3000
Crossover fcn.	scattered
Crossover fraction	40%
Mutation operator	Gaussian
Mutation fraction	60 %
Elite count	0
Evaluation count	
Time used	4 hours

TABLE XII
INPUT DATA FOR GA-MEC FOR FLUX BARRIERS

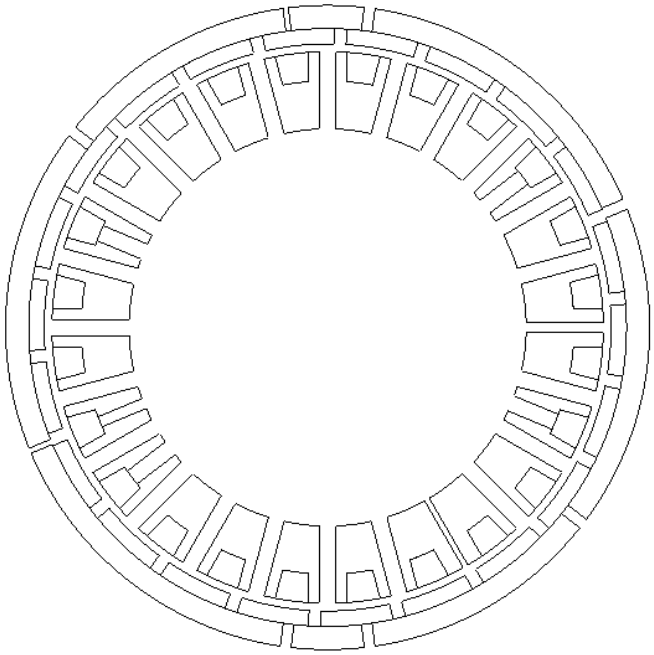

Fig. 42. GA-MEC solution. Width of air gaps are 7,14 or 21 mm. Single layer winding.

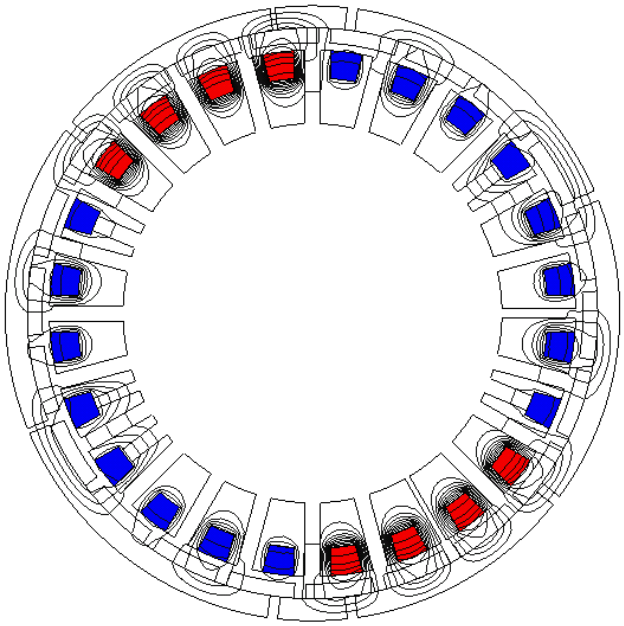

Fig. 43. GA-MEC solution. Flux line plots. Width of air gaps are 7,14 or 21 mm. Single layer winding. Colors indicate current. red 1.0 pu, blue -0.5 pu.

shows the flux lines when current are applied to the single layer winding. The air gap flux density is seen in Fig. 44 along with the corresponding spectrum in Fig.40.

1) Transient simulation: Results from the transient simulation are seen in Table VI. With equal

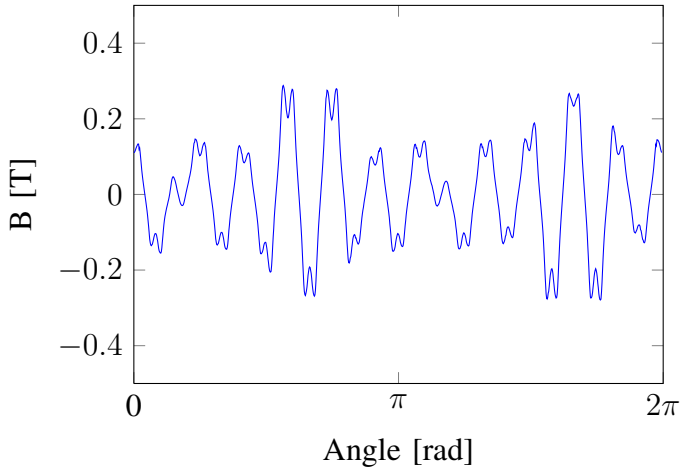

Fig. 44. Air gap flux density plot for GA-MEC solution. Horizontal axis equal zero at the positive x axis Fig. 43.

armature excitation as the ordinary single layer case the output torque where reduced. Flux density in the stator teeth's are 1.8 T, causing saturation. The ripple torque has increased to the ordinary single layer machine.

VI. Discussion

A. Single layer

The single layer winding gives the simplest practical solution among the ones analysed, it is an easy to manufacture and assembly solution. In addition, as seen from Fig. 8, separation between phases gives a redundant machine in case of insulation degradation. Another characteristic concerning fault tolerance is the low mutual inductance. Table IV shows an uneven mutual inductance between the phases due to flux density harmonics, albeit they are low valued compared to other solutions. Consequently a short circuit in one phase has low impact on the performance of the other phases.

Although the simplicity and high winding factor in a 24 slot 22 pole machine, single layer layout presents high amount of sub-harmonics as seen in Fig. 31. Especially noticeable are the fundamental harmonic with 90 % amplitude of the main harmonic. Fig. 25 illustrates the excess flux created by the sub-harmonic, with the fundamental spanning 24 slot pitches, and the other harmonics traversing fewer slot pitches.

Despite the high current loading, flux from the magnets have higher amplitude thus reducing the relative amount of sub-harmonics present during operation.

Table VI compares the different winding layouts, verifying that the single layer winding presents the highest losses. With eddy currents in the rotor and magnets being the most pronounced source.

B. Double layer

The double layer winding complicates the winding layout. Each slot now shares two coils of same phase or different phase as seen in Fig. 13 and Fig. 14. Consequently, making the machine prone to loss of performance in case of a insulation fault, giving a less redundant solution than the single layer.

As with single layer, the double layer winding gives a low mutual inductance in favour of fault operation. Table V gives the inductances with 60 turns per coil, however with the dimensional constrains, a 60 turn coil would not be feasible, thus a reduced number of turns or reduced conductor gauge would impact the inductances. Regardless, mutual inductance is low and equal for all phases due to reduced sub-harmonics.

Fig. 31 gives the harmonic content of the double layer winding showing a fundamental with 17 % amplitude compared to the main harmonic. A 83 % reduction compared to the single layer. The 5.th and 7.th harmonic sees a reduction of 34 % and 18 % respectively. In turn, the main harmonic gives a higher amplitude per A-turn possibly reducing the winding losses.

Comparing Fig. 25 and Fig. 29 the reduction in fundamental harmonic is apparent. More flux passes one pole pitch creating a stronger working torque.

Table VI state a 46.4 % reduction in solid and core losses compared to the single layer. In particular eddy current losses in the rotor yoke is reduced, possibly being a consequence of reduced sub-harmonics.

Although single layer winding presented a high winding factor for the 24 slot 22 pole ($q = 4/11$) machine, double layer winding does not present a high winding factor. Other slot/pole combinations may want to be revised in order to increase the winding factor.

C. Four Layer

Along with the solutions above the four layer winding presents the last analytical approach using

the star of slots. Increased degrees of freedom in coil placement indicate a further reduction in sub-harmonics.
As noticed in Fig. 15 and Fig. 16 the four layer, in practice a three layer, further complicates the assembly of the winding layout. From these, and Fig. 11 it is apparent that this configuration would increase the mutual inductance between the phases making the machine prone to performance reduction during fault operation. The increased mutual inductance is observed in Table VII, assuming 60 turn coils. With the dimensional constrains on the number of turns , inductance may be reduced.
Fig. 31 disclose a 28 % increase in the fundamental harmonic compared to the double layer. A increase is also observed for the 5.th harmonic were as the 7.th harmonic sees a 79 % reduction in amplitude compared to the double layer. The 5.th harmonic is noticeable in Fig. 32 were the flux spans more than one pole pitch.
Total losses associated with the four layer winding is seen in Table VI with a 155 W reduction compared to the double layer is observed. Considering the fundamental harmonic and 5.th harmonic increased compared to the double layer losses, the amplitude of the 7.th harmonic seems to have a impact on the losses.

D. GA Double Layer

The Genetic Algorithm with double layer constraints produced a winding similar to the ordinary double layer, except for different number of turns on each coil. Consequently increasing the complexity of production and assembly.
As with the ordinary double layer the mutual inductance is low, seen in Table. VIII, giving a more fault tolerant machine. Although physical separation between the phases does not exist as with the single layer winding.
Observing the harmonic spectrum in Fig. 31, a 13 % decrease in the fundamental and a 59 % reduction in the 5.th harmonic compared to the ordinary double layer is observed. Were as the 7.th harmonic sees a 36 % increase from the ordinary double layer.
Losses associated with the winding layout is close to the ordinary double layer winding as seen in Table VI. However, ripple torque is 67 % higher than the ordinary double layer winding, possibly stemming from the uneven number of turns of each coil. The increased complexity and torque ripple along with no reduction in losses, votes in disfavour of choosing this winding layout over the ordinary double layer winding.
Regarding the performance of the GA, the fixed amount of generations computed with no convergence criteria gave a computation time of 11 hours. The final solution was found in fewer generations due to elitism. Consequently, convergence and stall criteria would decrease the computation time. Another source of long computation time was the custom mutation and crossover functions constructed to obey the constraints. Conditional statements checking the feasibility of gene placement is time consuming, and the use of linear constraints and repair algorithms might performed faster.

E. GA Four Layer

The GA Four layer solution is the most complex winding layout presented, considering the different number of turns on each coil, and the number of coils in each slot.
As noticed from the idealized MMF in Fig. 12 the mutual inductance between the phases is high, verified in Table IX. Inductance values assumes the number of turns are in the range of 44 to 153, which in practice is not feasible due to dimensional constraints. However mutual inductance impacts the performance during fault operation.
Fig. 31 exhibits a complete reduction of sub-harmonics, completing the objective in the problem statement. Although, the winding factor is low compared to the single and double layer, making this a object for further research.
Total solid losses, reported in Table VI, are 1.44 kW. A 63 % reduction in losses compared with the single layer, and a 31 % reduction from the double layer winding. Results indicating a more energy efficient machine, albeit more complex. The average torque are 7.47 kNm and with a torque ripple of 66 Nm, the lowest ripple torque among the winding solutions analysed.
Regarding performance of the algorithm, a no constrained problem produce a fast algorithm making it possible to increase the population size. Yielding a better coverage of the solution space. Given the large population and number of generations it is believed that a close to global optimum, w.r.t. the fitness functions, is found.

Different input parameters showed elitism produces a faster convergence, thus reducing the search space. Likewise, uniform mutation proved less successful regarding covering the search space. Crossover fraction in the range of 0.5 proved efficient giving a good convergence progress and coverage of the solution space. A higher fraction produced to fast a convergence and a local optimum solution.

F. Flux Barrier: 6+6 sectioning

The 6+6 sectioning of the stator demonstrated promising results decreasing the fundamental harmonic. With a 4 mm air gap the fundamental harmonic decreased with 44 %, without affecting the main harmonic. Likewise, the 5.th harmonic saw a 39 % decrease in amplitude, were as the 7.th harmonic saw little change as seen in Fig. 40. A larger width of the air gap could further decreased the sub-harmonic content.

G. Flux Barrier: GA-FEM

Optimization of Flux Barriers using FEA software proved difficulty. Interfacing two software's was time consuming, possible due to the technique chosen. Other techniques and software's might show greater potential, being a topic of further researched. 10 generations with a population size of 25 individuals took 3.5 hours to complete. Neither the population size nor the number of generations are high enough to suggest this is a global optimum. Ergo larger population size and generation number are advised in future analysis.
Fig. 41 displays the variation the algorithm converged to, and obviously flux barriers are optimized w.r.t the flux at time equal to zero. At other instants of time the sub-harmonic flux takes another path, rendering the flux barriers placement less optimal.
As a result of long computation time and the low population and generation size, giving a low coverage of the solution space, a Magnetic Equivalent Circuit (MEC) where used instead of FEA.

H. Flux Barrier: GA-MEC

MEC gives a set of linear algebraic equations, faster to solve than post and pre-processing in FEA, subsequently a larger population size is used, giving a better coverage of the solution space.
The inaccuracy in neglecting the location of the magnets made the position of the flux barriers in the rotor unsymmetrical. Secondly, the width of the flux barrier made the area of each tooth smaller, causing saturation and a reduction of the main harmonic flux. Consequently, neglecting the reluctance of the stator and rotor yokes caused the solution to converge on the solution seen in Fig. 42.
Fig. 40 indicates a reduction of 92 % in the fundamental harmonic. Were as the 5.th harmonic saw a 67 % reduction compared to the ordinary single layer case. The 7.th harmonis saw no change in amplitude.
A concern with flux barriers are the ripple torque created by the changing flux path. FEA calculation revealed a ripple torque with peak to peak value of 774 Nm, a 470 % increase from the ordinary single layer machine. Were as the average torque are reduced to 6.2 kNm, originating from the increased reluctance for the main harmonic.
The total computed losses were 2.45 kW, a 38 % reduction in losses compared to the ordinary single layer case. However the output torque is reduced not giving a good comparison of the efficiency. By increasing the A-turn to achieve the required torque, increases the eddy current losses and winding losses, reducing the difference in losses.
A more practical solution would be a smaller width of the flux barriers. Likewise the flux barriers in the rotor could be ignored.
Further imposing constraints, improving model accuracy and objective functions could lead to a better solution with lower losses and less ripple torque.

VII. Conclusion

Fractional slot winding machines with concentrated coils are popular in applications demanding high torque, low volume and high fault tolerance. The special case of a 24 slot 22 pole machine with a single layer winding provides a high winding factor in contrast to other slot and pole combinations in the nearby range. But such a choice of slot and pole combinations with single layer winding exhibit high amount of sub-harmonic magnetic fields being a source of additional losses, giving a less efficient machine and developed more heat.
Solutions like increasing the number of layers, varying the number of turns on each coil and introducing flux barriers in the machines have been

proposed to reduce the amount of sub-harmonic fields. With the use of analytical approaches and numerical optimization procedures these solutions are implemented in an optimal way.

The analytical approach using the star of slots for two layer winding demonstrated a 83 % reduction in the fundamental harmonic compared to the single-layer winding. Consequently, the solid losses, excluding the winding losses, were reduced by 46 % giving a substantially better efficiency than the single-layer winding. Further, incrementing to fours layer exhibited little gain in efficiency, in addition to increasing the mutual inductance and increasing the complexity of the winding layout. The four layer winding is therefore a less favourable choice for the intended applications.

The second approach used Genetic Algorithms to optimize the winding layout. Genetic Algorithms are able to search a larger discontinuous solutions space than analytical approaches, increasing the probability of finding a more optimal solution. A two layer winding solution found by the Genetic Algorithm reported only a slight decrease in sub-harmonic contents compared to the ordinary two layer winding. In addition to increasing the complexity of the winding layout and lowering the winding factor but not decreasing the solid losses. Further research on increasing the winding factor and decreasing the sub-harmonic content is advised. A four layer winding produced by the Genetic Algorithm reported a complete removal of sub harmonics. Secondly, solid losses where reduced by 63 % compared to the single-layer winding. Lastly a reduction in ripple torque was achieved. However, the layout presented a low winding factor, a high mutual inductance, and complex winding layout, making it a choice for special applications where energy efficiency and low torque ripple is particular of interest.

The third approach uses flux barriers to indirectly influence the amount of sub-harmonics. A Genetic Algorithm is used to find the optimal arrangement of flux barriers in the 24 slot 22 pole machine using Finite Element Methods and Magnetic Equivalent Circuits.

Interconnecting Genetic Algorithms and Finite Element Analysis suggested a proved performance in computation time, in addition, the algorithms converged on a solution not assessing the time and rotational aspect of the machine.

A Magnetic Equivalent Circuit decreased the computation time, allowing the algorithm to cover a larger solution space finding a more optimal solution. The proposed solution gives a 38 % reduction in solid losses compared to the ordinary single layer case. However, a decrease in output torque and a 470 % increase in ripple torque are reported. This makes the solution a poor choice in low ripple application. Further work on reducing the ripple torque by improving the MEC model and fitness functions in the GA should be done.

Genetic Algorithms display great potential in machine design optimization due to the discontinuous nature of the solution space. Traditional line search methods may fail in finding a non-local optimum, making the need for multiple starting points, consequently increasing the computation time. Whereas the Genetic Algorithms starts with a wide search of the solution space making it more prone to finding a global optimum. However, using Genetic Algorithms in connection with computationally demanding problems increases the computation time due to the number of function evaluations needed to cover the solution space, and as a result the number of variables must be decreased.

VIII. Further work

This report did not take into account the physical restrictions on the winding layout. A further investigation on practical realisation with regards to number of turns on each coil, the placement of coils in the top and bottom layers and the resulting winding losses is of interest. Also generator operation and regenerative breaking properties would be of interest including operation with traditional drives systems.

Flux barriers presented large ripple torque, further research on implementation and optimization of flux barriers with the objective to reduce the ripple torque should be performed. Further developing the Magnetic Equivalent Circuit by including the reluctances of stator and rotor yoke, the magnets placement and excitation and torque production. Added time-steps to include rotational effects and developing objective functions taking into account ripple torque would present better model accuracy resulting in the GA finding a more optimal solution than presented.

Different approaches using GA interfaced with FEA

software should be investigated. Either by further developing the approach proposed, or use other FEA softwares with better interface to Matlab or other optimization tool. Comsol Multiphysics presents a promising solution having a functional interface with Matlab. In addition further develop the objective/fitness functions accounting for ripple torque and rotational effects.

Calculating core losses in rotor and stator with respect to harmonic flux densities would further increase the accuracy of power loss calculations. With the core loss calculations presented here, harmonics and distorted flux density waveforms are not modelled correctly. Implementing correction factors for distorted waveform could be done, however measurements should be performed to verify and validate the new approach.

Further improvement in fitness functions for the double and four layer winding GA may present solutions with higher winding factors than the one proposed. A second approach would be to impose constraints on the layout with the objective to obtain a higher winding factor. Third, investigate other slot/pole combinations presenting higher winding factor for the ordinary double and four layer winding, increasing the probability of finding a solution with higher winding factor. Further research is highly advised.

Lastly, an improvement in computation speed for the double layer GA would decrease the computation time during optimization. Either with the use of new chromosome string representation along with new custom operators, or using linear or non-linear constraints with repair or penalty functions. Comparing the two algorithms regarding convergence speed and optimal solution would indicate the preferred choice of algorithm in future optimization.

REFERENCES

[1] Z. Michalewicz, *Genetic Algorithms + Data Structures = Evolution Programs*. Springer-Verlag, 1996.

[2] A. Smith and D. Delgado, "Automated ac winding design," in *Power Electronics, Machines and Drives (PEMD 2010), 5th IET International Conference on*, 2010, pp. 1–6.

[3] J. Mayer, G. Dajaku, and D. Gerling, "Mathematical optimization of the mmf-function and -spectrum in concentrated winding machines," in *Electrical Machines and Systems (ICEMS), 2011 International Conference on*, 2011, pp. 1–6.

[4] G. Dajaku and D. Gerling, "A novel 12-teeth/10-poles pm machine with flux barriers in stator yoke," in *Electrical Machines (ICEM), 2012 XXth International Conference on*, sept. 2012, pp. 36 –40.

[5] Ø. Krøvel, "Design of large permanent magnetized synchronous electric machines : Low speed, high torque machiines - gererator for diriect driven wind turbine- motor for rim driven thruster," Ph.D. dissertation, Norwegian University of Science and Technology, Department of Electrical Power Engineering, 2011.

[6] N. Bianchi, S. Bolognani, M. Pre, and G. Grezzani, "Design considerations for fractional-slot winding configurations of synchronous machines," *Industry Applications, IEEE Transactions on*, vol. 42, no. 4, pp. 997 –1006, july-aug. 2006.

[7] T. Jahns, "Improved reliability in solid-state ac drives by means of multiple independent phase drive units," *Industry Applications, IEEE Transactions on*, vol. IA-16, no. 3, pp. 321–331, 1980.

[8] A. Jack, B. Mecrow, and J. Haylock, "A comparative study of permanent magnet and switched reluctance motors for high-performance fault-tolerant applications," *Industry Applications, IEEE Transactions on*, vol. 32, no. 4, pp. 889–895, 1996.

[9] G. Bertotti, "General properties of power losses in soft ferromagnetic materials," *Magnetics, IEEE Transactions on*, vol. 24, no. 1, pp. 621–630, 1988.

[10] P. Rasilo, D. Singh, A. Belahcen, and A. Arkkio, "Iron losses, magnetoelasticity and magnetostriction in ferromagnetic steel laminations," *Magnetics, IEEE Transactions on*, vol. 49, no. 5, pp. 2041–2044, 2013.

[11] C. Graham, "Physical origin of losses in conducting ferromagnetic materials (invited) a)," *Journal of Applied Physics*, vol. 53, no. 11, pp. 8276–8280, 1982.

[12] J. Lavers, P. Biringer, and H. Hollitscher, "A simple method of estimating the minor loop hysteresis loss in thin laminations," *Magnetics, IEEE Transactions on*, vol. 14, no. 5, pp. 386–388, 1978.

[13] M. K. Jamil and N. Demerdash, "Harmonics and core losses of permanent magnet dc motors controlled by chopper circuits," *Energy Conversion, IEEE Transactions on*, vol. 5, no. 2, pp. 408–414, 1990.

[14] E. Spooner, A. Williamson, and G. Catto, "Modular design of permanent-magnet generators for wind turbines," *Electric Power Applications, IEE Proceedings* -, vol. 143, no. 5, pp. 388–395, 1996.

[15] *Mathworks, Matlab, Global Optimization Toolbox*. [Online]. Available: http://www.mathworks.se/help/gads/genetic-algorithm.html

[16] D. Haupt, R.and Werner, *Genetic Algorithms in Electromagnetics*. Wiley-IEEE Press, 2007.

[17] L. Alberti and N. Bianchi, "Theory and design of fractional-slot multilayer windings," *Industry Applications, IEEE Transactions on*, vol. 49, no. 2, pp. 841–849, 2013.

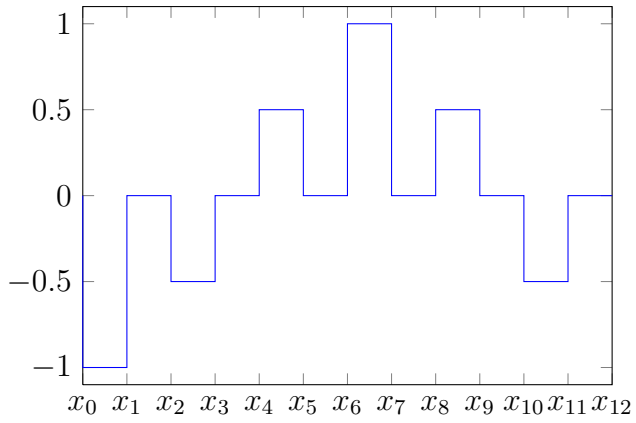

Fig. 45. MMF from a single layer 12 slot 10 pole machine. Used in calculations of harmonics

APPENDIX A
FOURIER SERIES DERIVATION

A. Introduction

Fourier series are a mathematical method for approximation of a signal by the use of sine and cosine terms. It is defined as:

$$f(x) = \frac{a_0}{2} + \sum_{n=1}^{\infty} \left(a_n \cos \frac{2n\pi x}{X} + b_n \sin \frac{2n\pi x}{X} \right) \tag{15}$$

where the coefficient, a_n and $b_n$are given by:

$$a_0 = \frac{2}{X} \int_0^X f(x)dx \tag{16a}$$

$$a_n = \frac{2}{X} \int_0^X f(x) \cos \frac{2n\pi x}{X} dx \tag{16b}$$

$$b_n = \frac{2}{X} \int_0^X f(x) \sin \frac{2n\pi x}{X} dx \tag{16c}$$

Fourier series are used in analysing the harmonic content in the magnetomotive force produced by the winding. Fig.45 shows a the air gap MMF at time equal to zero (t=0) with symmetric currents applied. That is:

$$I_a = Icos(2\pi ft)$$
$$I_b = Icos(2\pi ft - \frac{2\pi}{3})$$
$$I_c = Icos(2\pi ft + \frac{2\pi}{3})$$

Noting that:

$$tw = x_k - x_{k+1} \qquad \text{when } k = \text{even}$$
$$sw = x_k - x_{k+1} \qquad \text{when } k = \text{odd}$$

where tw and sw are tooth width and slot width respectively.

B. Dependencies

Solving (16) for the coefficient in the above MMF we get:

$$a_n^v = \frac{I}{\pi n} \left[\sin \frac{2\pi nx}{X} \right]_{x_k}^{x_{k+1}}$$
$$b_n^v = \frac{-I}{\pi n} \left[\cos \frac{2\pi nx}{X} \right]_{x_k}^{x_{k+1}}$$

where c equal 1 or 2.

C. In polar coordinates

Fourier series can be extended to polar form, where the variable x [mm] is changed to θ. Then, $X = 2\pi r$ is converted to the circumference of the air-gap. And the arc length of the slots and tooth's $(x_0, x_1, x_2\ etc.)$ are given as $x_k = \theta_k r$, e.g. $x_1 = \theta_1 r$. Where r is the radius of the air-gap. Inserting these into the above equations one get:

$$a_n^v = \frac{I}{\pi n} \left[\sin \frac{2\pi nx}{2\pi r} \right]_{\theta_k r}^{\theta_{k+1} r} \tag{18a}$$

$$b_n^v = \frac{-I}{\pi n} \left[\cos \frac{2\pi nx}{X} \right]_{\theta_k}^{\theta_{k+1} r} \tag{18b}$$

Expanding (18) we get:

$$a_n^v = \frac{I}{\pi n} \left[\sin \frac{2\pi n\theta_{k+1} r}{2\pi r} - \sin \frac{2\pi n\theta_k r}{2\pi r} \right] \tag{19a}$$

$$b_n^v = \frac{-I}{\pi n} \left[\cos \frac{2\pi n\theta_{k+1} r}{2\pi r} - \cos \frac{2\pi n\theta_k r}{2\pi r} \right] \tag{19b}$$

Removing the terms that cancels gives:

$$a_\nu^v = \frac{I}{\pi \nu} \left[\sin \nu\theta_{k+1} - \sin \nu\theta_k \right] \tag{20a}$$

$$b_\nu^v = \frac{-I}{\pi \nu} \left[\cos \nu\theta_{k+1} - \cos \nu\theta_k \right] \tag{20b}$$

From now on: n is replaced by ν for the harmonic order.

The above expression tells the contribution from each column in fig. 45 to the different harmonics. The last term in the square brackets in 20 can be simplified by use of identities:

$$\theta_{tw} = \theta_{k+1} - \theta_k \qquad \text{when } k = \text{even} \tag{21a}$$

$$\theta_{sw} = \theta_{k+1} - \theta_k \qquad \text{when } k = \text{odd} \tag{21b}$$

Hence the angle θ_{tw} and θ_{sw} is constant yielding a "phase shift" between the two sinusoids. Thus the term in the square brackets can be thought of as a sum of sinusoids with a phase shift.

D. Matrix form of complex Fourier series

The standard Fourier series contains sum of sine and cosine terms, using Eulers relations these terms can be expressed in complex numbers. With the use of:

$$\begin{aligned}\exp \pm j\theta &= \cos\theta \pm j\sin\theta \\ \cos\theta &= \tfrac{\exp j\theta + \exp -j\theta}{2} \\ \sin\theta &= \tfrac{\exp j\theta - \exp -j\theta}{2}\end{aligned}$$

The Fourier representation:

$$f(t) = \frac{a_0}{2} + \sum_{n=1}^{\infty}\left(a_n \cos\frac{2n\pi t}{T} + b_n \sin\frac{2n\pi t}{T}\right)$$

$$f(t) = \frac{a_0}{2} + \sum_{n=1}^{\infty}\Big(\frac{a_n - jb_n}{2}\exp(j2n\pi t/T) \quad (22)$$

$$+ \frac{a_n + jb_n}{2}\exp(j2n\pi t/T)\Big) \quad (23)$$

$$f(t) = \sum_{n=-\infty}^{\infty} c_n \exp(j2n\pi t/T) \quad (24)$$

Where

$$\begin{aligned}c_n &= \frac{a_n - jb_n}{2} \\ c_{-n} &= \frac{a_n + jb_n}{2} \\ n &= 1, 2, ...\end{aligned}$$

$$c_n = \frac{1}{T}\int_0^T f(t)\exp(-j2n\pi t/T)dt \quad (25)$$

Converting to polar form we get:

$$\begin{aligned}c_n &= \frac{1}{2\pi r}\int_0^{\theta r} f(\theta r)\exp(-j2n\pi\theta r/2\pi r)d(\theta r) \\ &= \frac{1}{2\pi}\int_0^{\theta} f(\theta)\exp(-jn\theta)d(\theta)\end{aligned}$$

Solving the integral, and remembering that $f(\theta)$ is piecewise we get:

$$c_n = \frac{j}{2\pi n}\left[f(\theta)\exp(-jn\theta)\right]_{\theta_i}^{\theta_i+\theta_{tw}} \quad (26)$$

Using (26) to evaluate the MMF in the first figure we see that it can be expressed in matrix form as:

$$\mathbf{c}^T = A\mathbf{f}^T \quad (27)$$

where the coefficient of matrix A(a_{nj}) is given by:

$$a_{ni} = \frac{1}{2\pi}\int_0^{\theta} f(\theta)\exp(-jn\theta)d(\theta) \quad (28)$$

$$= \frac{j}{2\pi n}\Big[f(\theta)\exp(-jn\theta)\Big]_{\theta_i}^{\theta_i+\theta_{tw}} \quad (29)$$

Another simplification: Taking (23) and noticing that c_{-n} is the complex conjugate of c_n we can write:

$$f(t) = \frac{a_0}{2} + \sum_{n=1}^{\infty}\left(c_n\exp(j2n\pi t/T) + c_n^*\exp(j2n\pi t/T)\right) \quad (30)$$

c_n is another complex vector, we can write:

$$f(t) = \frac{a_0}{2} + \sum_{n=1}^{\infty}\Big(\exp(j\phi)\exp(j2n\pi t/T) \quad (31)$$

$$+ \exp(-j\phi)\exp(-j2n\pi t/T)\Big) \quad (32)$$

Giving:

$$f(t) = \frac{a_0}{2} + \sum_{n=1}^{\infty}\Big(\exp(j2n\pi t/T + \phi) \quad (33)$$

$$+ \exp(-j2n\pi t/T - \phi)\Big) \quad (34)$$

Eulers relations gives:

$$a\cos(wt+\phi) = \frac{1}{2}a\exp(jwt+\phi) + \frac{1}{2}a\exp(-jwt-\phi) \quad (35)$$

Comparing (34) and (35) we get:

$$f(t) = \frac{a_0}{2} + \sum_{n=1}^{\infty}\left(2\ \text{abs}(c_n)\cos(2n\pi t/T + \phi)\right) \quad (36)$$

where $\phi = \text{angle}(c_n)$
In the initial analysis only the amplitude of each harmonic is of interest, hence we are interested in the term:

$$2\ \text{abs}(c_n) =$$

$$2\ \text{abs}\left(\frac{1}{2\pi}\int_0^{\theta} f(\theta)\exp(-jn\theta)d(\theta)\right)$$

Since the MMF is piece-wise, the integral must be expanded to all thoots (Q). This is best be performed in matrix form.

The above integral results in solutions in the form (for each tooth):

$$\frac{1}{2\pi}\int_0^{\theta} f(\theta)\exp(-jn\theta)d(\theta) \propto \frac{j}{2\pi n}\left[f(\theta)\exp(-jn\theta)\right]_{\theta_i}^{\theta_i+\theta_{tw}}$$

$$\frac{jf(\theta_i)}{2\pi n}\left[\exp(-jn(\theta_i+\theta_{tw}) - \exp(-jn\theta_i)\right] =$$
$$\frac{jf(\theta_i)}{2\pi n}\left[\exp(-jn\theta_i)\exp(-jn\theta_{tw}) - \exp(-jn\theta_i)\right] =$$
$$\frac{jf(\theta_i)}{2\pi n}\left[\exp(-jn\theta_i)\Big(\exp(-jn\theta_{tw}) - 1\Big)\right]$$

Where $\exp(-jn\theta_{tw}) - 1 =$ constant for all tooths, and $\exp(-jn\theta_i)$ is a phasor with constant increase in angle going around the whole circumference of the stator. That is, $\exp(-jn\theta_{tw}) - 1$ only introduces a amplitude increase/decrease and phase shift when multiplied with $\exp(-jn\theta_i)$.

The equation used in the calculating the harmonics are (27) and where $\mathbf{f}$ is a vector of the amplitude of the MMF in each slot. The final magnitude magnitude of the harmonics are $2\ abs(\mathbf{c})$.

APPENDIX B
GA DOUBLE LAYER CODE

Contents


```
function [ z ] = FitnessFunctionFourLayer( x )

%Fitness function for four layer winding layout
% x is a string of each individual
% x=[height tooth 1, height tooth 2, ..., ]
% Bound is -1 to 1
p=11;   %Pole pair
Q=24;   %Slot number
numberOfHarmonics=20;
[PopulationSize, genomeLength]=size(x);
%Transformation matrix
A=[1:1:Q ; 9:1:Q 1:1:8; 17:1:Q 1:1:16]';

phA=x;
phB(A(:,2))=phA*-0.5;   %MMF from phase B winding
phC(A(:,3))=phA*-0.5;   %MMF from phase C winding

MMF=phA+phB+phC;    %Total MMF

tw=ones(1,Q).*2*pi/Q;   %Angle of tooth in sucsessive order
t=(0:1:Q-1).*2*pi/Q;    %Angle of each slot

n=transpose(1:1:numberOfHarmonics);
B=zeros(numberOfHarmonics,Q);       %Matrix used in Fourier series calulation
for j=1:Q
    B(:,j)=1i./(2*pi.*n).*(exp(-1i.*n.*(t(j)+tw(j)))-exp(-1i.*n.*t(j)));
end

FComplex=B*transpose(MMF);

F=2*abs(FComplex);    %Magnitude of each harmonic
```

Computing partial fitness values

```
Z1= sum(F(1:p-1,:).^2,1) ./ F(p,:).^2 ; %First partial fitness function

Z2= ( F(p,:).*F(p-1,:) ) ./ ( 0.25*(F(p,:)+F(p-1,:)).^2 ) ; %Second partial fitness function

%highestOrder=5+p;
highestOrder=numberOfHarmonics;
n=p+1:1:highestOrder;
divisor=repmat(((n-p).^2)',1,PopulationSize);
intermediate= F((p+1):highestOrder,:).^2 ./divisor ;
Z3= sum(intermediate,1) ./ F(p,:).^2 ;                  %3.th partial fitness function
%
%Winding factor
k=1:1:Q;
%t=gcd(Q,p);
alpha=2*pi*t/Q;     %Angle between two adjecent slots
kTooth=abs(cos(alpha/2)); %Winding factor due to concentrated coils
E=exp(1i*2*pi*p*k/Q);   %Vector

geometricSumAbs=abs(phA*E');     %Resulting vectors
```

```
arithmeticSum=sum(abs(phA),2);    %Sum along rows

kw=geometricSumAbs*kTooth./arithmeticSum;

Z4=(1-kw').^2; %4.th partial fitness function


k1=1; k2=1; k3=1; k4=1;
Z=k1*Z1 + k2*Z2 + k3*Z3 + k4*Z4;

z=transpose(Z); %Return as column vector.

end
```

APPENDIX C
GA DOUBLE LAYER CODE

A. Fitness function

```
function [ z ] = FitnessFunction5_4( x )
%Version 5.4
%
% GA algorithm minimizes the fitness function
% We try to optimize with respect to 11 harmonic
% Uses vectorized form that is x is the entire population?

%Input: x is a matrix of the population. Rows are each entity in the
%population. Coulmns are the genes of that entity
% Genes are a number from 1 to Q*layers describing which phasor the phase is assigned.

% Initial values (can be changed using anonymus functions)
   global p
   global Q
   global m
   global layers

numberOfHarmonics=20;   %number of harmonics computed
numberOfLayers=layers;       %Layers

%

[PopulationSize, nVariables]=size(x);

GenomeLength=nVariables;

tw=ones(1,Q).*2*pi/Q;   %Angle of tooth in sucsessive order
t=(0:1:Q-1).*2*pi/Q;    %Angle of each slot

n=transpose(1:1:numberOfHarmonics);
A=zeros(numberOfHarmonics,Q);       %Matrix used in Fourier series calulation
for j=1:Q
    A(:,j)=1i./(2*pi.*n).*(exp(-1i.*n.*(t(j)+tw(j)))-exp(-1i.*n.*t(j)));
end
%
toothTurns=zeros(PopulationSize,Q); %Zero matrix equal to population size and slots

% New
```

```
% Add the two other phases
phAidx=x(:,1:GenomeLength/2);
[phBidx,phCidx]=SelectPhaseBandC5_1(phAidx);

MMF=zeros(PopulationSize,Q);
phaseA=x(:,GenomeLength/2+1:GenomeLength);

phaseB=x(:,GenomeLength/2+1:GenomeLength);

phaseC=x(:,GenomeLength/2+1:GenomeLength);

phA=zeros(PopulationSize,Q);
phB=zeros(PopulationSize,Q);
phC=zeros(PopulationSize,Q);

    for k=1:PopulationSize

        phA(k,phAidx(k,:))=phaseA(k,:);
        phB(k,phBidx(k,:))=phaseB(k,:).*-0.5;
        phC(k,phCidx(k,:))=phaseC(k,:).*-0.5;

    end

MMF=phA+phB+phC;
%

TransToothTurns=transpose(MMF);     % Transpose the population since rows are equal to coulmn

Fcomplex=A*TransToothTurns;            % The resulting harmonic spectrum for the whole popula
                                % row are equal to the harmonic order
                                % columns are equal to the entity in population
                                % Is in complex form
F=2*abs(Fcomplex);                        %Take absolute value
% First objective function
% The magnitude of all harmonics below the working harmonic

Z1= sum(F(1:p-1,:).^2,1) ./ F(p,:).^2 ;     %Return a row vector
                                            % column are respectivly member
                                            % of population
% Second objective function
% optimize with respect to adjacent harmonics

Z2= ( F(p,:).*F(p-1,:) ) ./ ( 0.25*(F(p,:)+F(p-1,:)).^2 ) ;

% Third objective function
% The magnitude of all harmonics up to m above the working harmonic
n=numberOfHarmonics;
divisor=repmat(((1:1:n-p).^2)',1,PopulationSize);
intermediate= F((p+1):n,:).^2 ./divisor ;
Z3= sum(intermediate,1) ./ F(p,:).^2 ;

% Fourth objective function
% Winding factor
zeta=2*pi*p*F(p,:)./(m*4*3);
Z4=(1-zeta).^2;
% Test objective function
%Optimize harmonic (p)
```

```
%Z5=-F(p,:);
a0=sum(MMF,2)';
Z6=a0.^2;

% Resulting fitness value
% The abowe four values are weighted differently and summed to give the
k1=1; k2=1; k3=1; k4=1; k5=1; k6=1;
Z=k1*Z1 + k2*Z2 + k3*Z3+ k4*Z4+ k6*Z6;

z=transpose(Z); %Return as column vector.

end
```

B. Crossover function

```
function [ xoverKids ] = CrossoverFunction5_4( parents, options, GenomeLength, FitnessFcn, ..
                                                unused, thisPopulation)
%Function for crossover for MMF winding
% Uses scattered crossover
%Input variables are:
%   - parents : Row vector of parents choosen by the selection function
%   - options : options structure
%   - nvars/GenomeLength   : number of variables
%   - FitnessFcn : Fitness function
%   - unused  : Placeholder not used ??
%   - thisPopulation : Matrix representing the current population. no. rows are
%   population size, no. columns are is number of variables

%Returns: xoverKids - the crossover offspring -  as a matrix whose rows
%correspont to the children, columns equal number of variables

%Scattered crossover. Up to this
% point the child has the genes of the first parent and after this point
% the genes of the second parent

% How many children to produce?
nKids = length(parents)/2;

xoverKids = zeros(nKids,GenomeLength);

% To move through the parents twice as fast as thekids are
% being produced, a separate index for the parents is needed
index = 1;

for k=1:nKids
    % get parents
    parent1 = parents(index);
    index = index + 1;
    parent2 = parents(index);
    index = index + 1;
    %First half of genome
    for j = 1:(GenomeLength/2)
        avail=availableToothsDouble( xoverKids(k,1:GenomeLength/2) );
        if(rand > 0.5)

            if thisPopulation(parent1,j)==avail
                xoverKids(k,j) = thisPopulation(parent1,j);
            elseif thisPopulation(parent2,j)==avail
```

```
                xoverKids(k,j) = thisPopulation(parent2,j);
            else
                xoverKids(k,j) = avail(randi(length(avail),1));
            end

        else
            if thisPopulation(parent2,j)==avail
                xoverKids(k,j) = thisPopulation(parent2,j);
            elseif thisPopulation(parent1,j)==avail
                xoverKids(k,j) = thisPopulation(parent1,j);
            else
                xoverKids(k,j) = avail(randi(length(avail),1));
            end
        end

    end
    % Second half of Genome
    for i=GenomeLength/2+1:GenomeLength
        if rand > 0.5
            xoverKids(k,i) = thisPopulation(parent1,i);
        else
            xoverKids(k,i) = thisPopulation(parent2,i);
        end
    end
end


end
```

C. Mutation function

```
function [ mutationChildren ] = MutationFunction5_4( parents, options, nvars,...
    FitnessFcn, state, thisScore, thisPopulation)
%Mutation function for optimizing winding layout
% Rev. 5.4
%

lower=-1;
span= 2;
GenomeLength=nvars;
mutationRate=0.01;   %Chance of genome being mutated. std=0.01

mutationPop=length(parents);
mutationChildren=zeros(mutationPop,GenomeLength);

for k=1:mutationPop
    %Vector of chromosome of a parent choosen by the selection function
    % (mutates only individes chosen by be selection function ? )
    child=thisPopulation(parents(k),:);
    % Gets the position of genes (in the parent in question) being mutated
    mutationPoints = find(rand(1,length(child)) < mutationRate); %array
    % each gene is replaced with a value chosen randomly from the range.

    %Mutates the indicies in the child with random number
    for j=1:length(mutationPoints)
    if mutationPoints(j) <= GenomeLength/2
            %Find available tooths for this parent
            childPass=child(1:GenomeLength/2); %Only first half
```

```
            childPass(mutationPoints(j))=[];   %Remove gene whos mutates
            avail = availableToothsDouble( childPass );
            child(mutationPoints(j)) = avail(randperm(length(avail),length(mutationPoints(j))
    else
        child(mutationPoints(j)) = lower + span*rand ;
    end
    end
    mutationChildren(k,:) = child;     %Saves in return matrix
end


end
```

D. Initial population function

```
function Population = InitialPopulation5_4(GenomeLength,FitnessFcn,options)
% This function returns the initial population
% for the problem where only the variables are the winding MMF.
% Uses Oridinal representation
% Uses a list of available tooths
% Notes and calculations in order to simplify overview
   global p
   global Q
   global m
   global layers
   PolePair=p;
   %
   lower=-1;
   span=2;

%
PopulationSize = sum(options.PopulationSize);  %Population size

%
Population=zeros(PopulationSize,GenomeLength);   %Population matrix

%  approach
for k=1:PopulationSize
     for j=1:GenomeLength/2
     avail = availableToothsDouble( Population(k,1:GenomeLength/2) );  %Find available tooths
     Population(k,j)=avail(randi(length(avail),1));     %Random tooths from available

     Population(k,GenomeLength/2+j)=lower+span*rand ;   %Random no. turns for that tooth

     end
end

end
```

E. Available tooth function

```
function [ avail ] = availableToothsDouble( x )
% Get tooth number, return the tooths that are available
% for double layer
 global Q
 Q=12;
 A=[1:1:Q; 9:1:Q 1:1:8 ;5:1:12 1:1:4]'; %Initial matrix
 if  isempty(x) || x(1)==0
```

```
     avail=unique(A);
 else
 % x might contain zeros
 zeroIndex=find(x==0);
 x(zeroIndex)=[];   %Remove the zeros
 % New approach
 taken=A(x,:);
 avail=1:1:Q;
 avail(taken)=[];


 end
end
```

APPENDIX D
GA - FEA

A. Main file

```
%GAMaxwell3

%This is the main file for running GA in Maxwell
%Uses bit string with two bits per flux barrier
%


global solved
global solution
global counter

noBit=2;
solved=zeros(2^(24),1);
solution=zeros(2^(24),1);
counter=1;

generations=50;
eliteCount=0;
crossFrac=0.5;
populationSize=25;

numberOfVariables=24*noBit;            %Number of variables
lower=0.004;
upper=0.010;

nvars=numberOfVariables;

options  = GAOptionsSetMaxwell3_0( Bound , populationSize,crossFrac,eliteCount );

% Start GA
tic
[x, fval, exitflag, output, population, scores] = ga(@FitMaxwell3,nvars,[],[],[],[],...
LB,UB,[],options);

time2=toc;
fprintf('%2.0f iterations took %5.2f seconds\n',populationSize*generations, time2);
```

B. Fitness function file

```
function [ fitVal ] = FitMaxwell3( x )
```

```
%Fitness function for flux barrier GA with Maxwell
% variable string is binary 0,1
%Script to run maxwell
% changes recorder VB script

%
global solved
global solution
global counter

noBit=2;
width=[7 14 21];
[popSize,genomeLength]=size(x);

fitVal=zeros(popSize,1);

iMaxwell = actxserver('AnsoftMaxwell.MaxwellScriptInterface');

Desktop = iMaxwell.GetAppDesktop();

Desktop.RestoreWindow;

Project = Desktop.SetActiveProject('FluxBarrierGA');

Design = Project.SetActiveDesign('matlab4');

Desktop.CloseAllWindows()
Editor = Design.SetActiveEditor('3D Modeler');

%The chromosome is such that two adjecent bits correspond to one flux
%barrier. 00 = 0mm, 10=7mm, 01=14mm 11= 21mm.
%tic;
for k=1:popSize

    % Check if variation is saved before
    variation=bi2de(x(k,:));
    idx=find(solved == variation,1,'first');

    if  isempty(idx)  %if empty solve variation

    solved(counter)=variation;


        for n=1:noBit:genomeLength-1

            pos=(n+1)/2;    %number of flux barrier in question
            %If gene equal to zero do
            if not( bi2de(x(k,n:n+1)) )
                string2='true';         %supress
            else
                string2='false';        %no not supress
            end

            if pos==24
                string1='Circle5:Subtract:2';
            else
                string1=strcat('FluxBarrier',num2str(pos),':Subtract:',num2str(pos+2) );
```

```
            end
            %Change the property of the flux barrier in question
            invoke(Editor,'ChangeProperty', {'NAME:AllTabs', {'NAME:Geometry3DCmdTab', ...
{'NAME:PropServers', string1}, {'NAME:ChangedProps', {'NAME:Suppress Command', 'Value:=',  ..
            string2}}}} );

            string3=strcat('NAME:FBW',num2str(pos));
            index=bi2de(x(k,n:n+1));
            if index==0
                index=1; %random, the flux barrier is suppresed anyway
            end
            value1=strcat(num2str(width(index)),'mm');

            invoke(Design,'ChangeProperty', {'NAME:AllTabs', {'NAME:LocalVariableTab', ...
  {'NAME:PropServers',  'LocalVariables'}, {'NAME:ChangedProps',...
              {string3, 'Value:=', value1}  }}} );
        end

        Design.Analyze('Setup1');

% Make report and get FFT

        Module = Design.GetModule('ReportSetup');

invoke(Module,'CreateReport', 'XY Plot 3', 'Fields', 'Rectangular Plot',  ...
  'Setup1 : LastAdaptive', {'Context:=', 'Circle14', 'PointCount:=', 1001}, {'Distance:=', {
  'All'}, 'r_R_out:=', {'Nominal'}, 'r_R_inner:=', {'Nominal'}, 'r_rotor_inner:=', { ...
  'Nominal'}, 'w_magnet:=', {'Nominal'}, 'r_rotor_outer:=', {'Nominal'}, 'a_magnet:=', { ...
  'Nominal'}, 'r_stator_outer:=', {'Nominal'}, 'r_stator_inner:=', { ...
  'Nominal'}, 'r_cooling_ring_inner:=', {'Nominal'}, 'N_turn:=', { ...
  'Nominal'}, 'Rotate:=', {'Nominal'}, 'Rotate2:=', {'Nominal'}, 'theta_current:=', { ...
  'Nominal'}, 'rotate3:=', {'Nominal'}, 'FBW1:=', {'Nominal'}, 'FBHeigth:=', { ...
  'Nominal'}, 'Test2:=', {'Nominal'}, 'FBW2:=', {'Nominal'}, 'FBW3:=', { ...
  'Nominal'}, 'FBW4:=', {'Nominal'}, 'FBW5:=', {'Nominal'}, 'FBW6:=', { ...
  'Nominal'}, 'FBW7:=', {'Nominal'}, 'FBW8:=', {'Nominal'}, 'FBW9:=', { ...
  'Nominal'}, 'FBW10:=', {'Nominal'}, 'FBW11:=', {'Nominal'}, 'FBW12:=', { ...
  'Nominal'}, 'FBW13:=', {'Nominal'}, 'FBW14:=', {'Nominal'}, 'FBW15:=', { ...
  'Nominal'}, 'FBW16:=', {'Nominal'}, 'FBW17:=', {'Nominal'}, 'FBW18:=', { ...
  'Nominal'}, 'FBW19:=', {'Nominal'}, 'FBW20:=', {'Nominal'}, 'FBW21:=', { ...
  'Nominal'}, 'FBW22:=', {'Nominal'}, 'FBW23:=', {'Nominal'}, 'FBW24:=', { ...
  'Nominal'}}, {'X Component:=', 'Distance', 'Y Component:=', {'BDot14'}}, {} );

        Module = Design.GetModule('Solutions');

        Module.FFTOnReport('XY Plot 3', 'Rectangular', 'mag');

        Module = Design.GetModule('ReportSetup');
        fileNameExport=strcat('C:/Users/thomnord/Documents/Ansoft/Scripts/Data/AirGapFFT',...
num2str(k),'.tab');

        Module.ExportToFile('FFT XY Plot 3',  fileNameExport);

        Module.DeleteAllReports
% Get file and calculate fitness value

        A = importdata(fileNameExport, '\t', 1);
            %A data is a structure format where A.data contains the data. column 1 is
```

```
            %harmonic order starting from 0 (DC), column 2 is the harmonics amplitude.
            %11. harmonic is row 12, 1. harmonic is row 2.

        p=11;
        F=A.data(2:12,2);  % 1. to 11.th
        F=F./F(p);
        no=transpose(1:1:10);
        z1=-A.data(12,2);
        %FirstHarm=A.data(2,2);
        %MainHarm=A.data(12,2);
        fitVal(k) = 10/F(p).* sum(F(1:p-1).^2 ./ no.^2 ) + z1 ;

        %fitVal(k)=FirstHarm./MainHarm;
        solution(counter)=fitVal(k);
        counter=counter+1;

    else
        fitVal(k)=solution(idx);
    end

end
%time=toc;

%fprintf('%2.0f iterations took %5.2f seconds\n',popSize, time);

delete(iMaxwell);

end
```

APPENDIX E
GA - MEC

A. Main file

```
%GA-MEC

%This is the main file for running GA in Maxwell
%Uses bit string with two bits per flux barrier
%

matlabpool local 12

noBit=2;
generations=5000;
eliteCount=0;
crossFrac=0.4;
populationSize=5000;

numberOfVariables=24*noBit*3;            %Number of variables
lower=0.004;
upper=0.010;

nvars=numberOfVariables;
LB=lower*ones(1,numberOfVariables);   %Lower bound;
UB=upper*ones(1,numberOfVariables);   %Upper bound;
Bound=[LB ; UB];                    %Bounds, (not used in binary string)

options  = GAOptionsGAMEC1_0( Bound , populationSize,crossFrac,eliteCount );
```

```
% Start GA
tic
[x, fval, exitflag, output, population, scores] = ga(@FitGAMEC1,nvars,[],[],[],[],LB,UB,[],op

time2=toc;
fprintf('%2.0f iterations took %5.2f seconds\n',populationSize*generations, time2);


matlabpool close
```

B. Fitness function file

```
function [ z4 ] = FitGAMEC1( x )
%Fitnes function for GA MEC

%Input are binary, must code to real value
I_peak= ? ;      %phase current
N_tunrns= ? ; %number of turns
F=sqrt(2)*I_peak*N_turns;
rotorThickness= ? ; %Rotor yoke thickness in millimeters [mm]
depth= ? ;          % Length of machine in axial direction [mm]
statorThickness= ? ;    %Stator thickness [mm]
toothThickness= ? ;     %Tooth thickness [mm]
mu0=4.*pi.*1e-7;        %Permeablimity of vacuum
lengthAirGap= ? ;       % Air gap length without magnets [mm]
muR=? ;                  % Relative permeability of flux barriers
toothWidth= ? ;         % Tooth width [mm]
%Reluctance of flux barriers in ...
RR=1e3./(mu0.*muR.*rotorThickness.*depth);  %...Rotor
RS=1e3./(mu0.*muR.*statorThickness.*depth); %...Stator
RT=1e3./(mu0.*muR.*toothThickness.*depth);  %...Tooth
RG=lengthAirGap./(mu0.*toothWidth.*depth).*1e3; %Air gap reluctance
widthBit=[0,7,14,21]; %in mm
Rg=RG;
%Rt=rand(1,48);
%Rr=rand(1,48);
%Rs=rand(1,48);
Rt=zeros(1,24);     %Rt are the first 24*noBit values in the string
Rs=zeros(1,24);     %Rs are the second 24*noBit
Rr=zeros(1,24);     %Rr are the third 24*noBit
counter=1;
for mm=1:2:24*2
    rotorBit=x(mm:mm+1);
    statorBit=x(mm+48:mm+48+1);
    toothBit=x(mm+96:mm+96+1);

    rotorIndex=bi2de(rotorBit)+1;
    statorIndex=bi2de(statorBit)+1;
    toothIndex=bi2de(toothBit)+1;

    Rr(counter)=RR*widthBit(rotorIndex);
    Rs(counter)=RS*widthBit(statorIndex);
    Rt(counter)=RT*widthBit(toothIndex);
    counter=counter+1;
end


phA=[1,-0.5,-0.5];  %Current in winding at three instances of times
```

```
phB=[-0.5,1,-0.5];
phC=[-0.5,-0.5,1];
fitVal=zeros(1,3);
z1=zeros(1,3);
c=Rg*ones(1,48-1);
d=-2*Rg*ones(1,48);
e=c;
A = gallery('tridiag',c,d,e); %System matrix without flux barriers

A(1,48)=Rg;
A(48,1)=Rg; %

n=1;
for k=1:2:48        % Matrix updated with flux barriers
    A(k,k)=A(k,k)-Rt(n);
    n=n+1;
end

n=1;
for k=2:2:48         % Matrix updated with flux barriers
    A(k,k)=A(k,k)-Rr(n)-Rs(n);
    n=n+1;
end

for m=1:3   % for three instances of time w=0, 2pi/3, etc.
    Va=F*phA(m);
    Vb=F*phB(m);
    Vc=F*phC(m);
b=zeros(1,48);
b(2)=-Va; b(4)=Va; b(6)=-Va; b(8)=-Vb; b(10)=Vb; b(12)=-Vb; b(14)=Vb;
b(16)=Vc; b(18)=-Vc; b(20)=Vc; b(22)=-Vc;

b(48)=Va; b(24)=-Va; b(26)=Va; b(28)=-Va; b(30)=Va; b(32)=Vb; b(34)=-Vb;
b(36)=Vb; b(38)=-Vb; b(40)=-Vc; b(42)=Vc;
b(44)=-Vc; b(46)=Vc;

xx=A\b';

g=[xx(48);xx(2:2:46)];
f=xx(2:2:48);
Flux=f-g;

%Fluxes is then multiplied with the Fourier series Matrix;
% Harmonic matrix (Fourier transform)
tw=ones(1,Q).*2*pi/Q;   %Angle of tooth in sucsessive order
t=(0:1:Q-1).*2*pi/Q;    %Angle of each slot
numberOfHarmonics=30;
n=transpose(1:1:numberOfHarmonics);
B=zeros(numberOfHarmonics,Q);       %Matrix used in Fourier series calulation
for j=1:Q
    B(:,j)=1i./(2*pi.*n).*(exp(-1i.*n.*(t(j)+tw(j)))-exp(-1i.*n.*t(j)));
end
%

avg=ones(1,24);
BB=[avg;B];
```

```
ComplexF=BB*Flux;    %First ones is the average value
                    %First harmonic start at index 2

absF=2*abs(ComplexF);

%stem(0:1:length(absF)-1,absF); %Plot spectrum


 p=11; % Harmonic to optimize w.r.t

%F=A.data(2:12,2);  % 1. to 11.th
F1=absF./absF(p+1); %Normalize to 11. harm
no=transpose(1:1:11);
z1(m)=absF(p+1);      %Maximize 11. harmonic

%The fitness value at one time on insant
%0.0031 is the refrence without flux barriers
fitVal(m) = 100*(1/F1(p+1).* sum(F1(1:p).^2 ./ no.^2 )) -1*z1(m)/(0.0031) ;

end

z2=abs(z1(1)-z1(2))+abs(z1(1)-z1(3))+abs(z1(2)-z1(3));
z2=z2*1e3;
z3=sum(fitVal);
z4=z2+z3;       %z4 is the final fitness value (return)

end
```